Application of RPCs for PET

Paolo Vitulo
Dipartimento di Fisica Nucleare e Teorica
Università di Pavia & INFN - Pavia –

Summary

- Introduction to PET
- Detectors
- Hardware description
- Software description
- Simulations and results
- Conclusions
- References

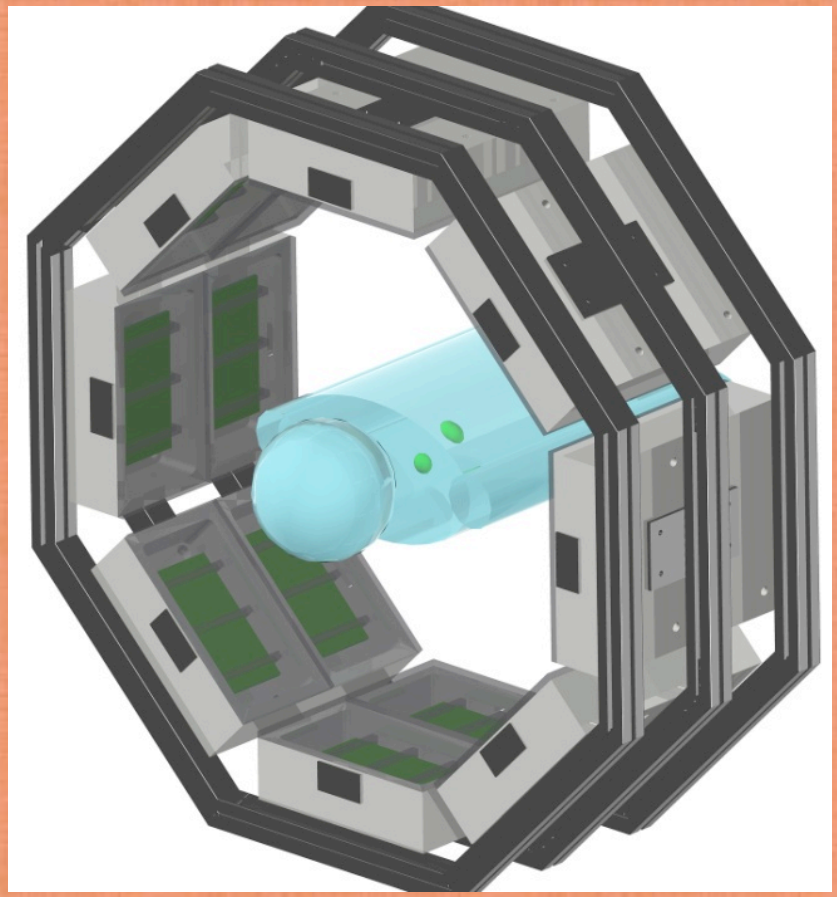

Positron Emission Tomography

Molecule of ^{18}F-Deoxyglucose

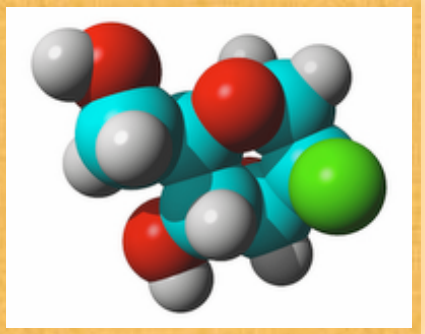

Imaging technique:

- Functional
- Non invasive

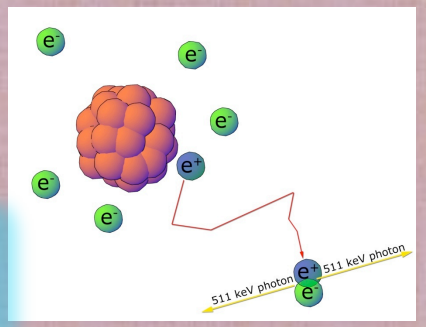

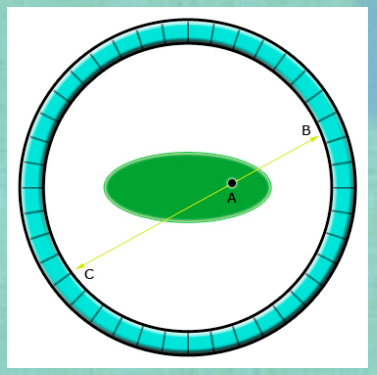

Basics:

- Labelled molecule
- Positron annihilation
- Gamma detection
- Data manipulation
- Image reconstruction

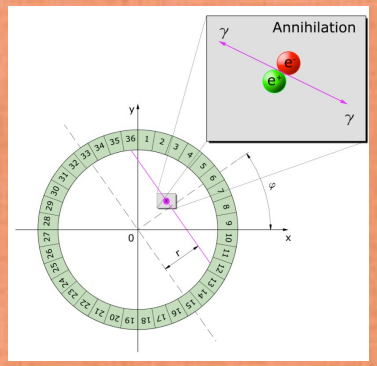

[Ame][Rad]

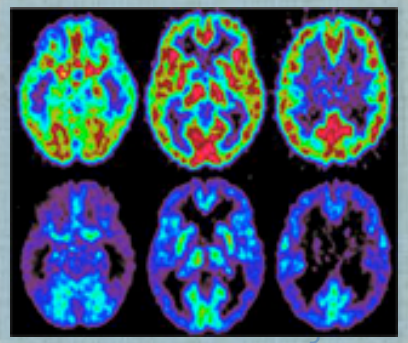

Radio-tracer

- Fluorodeoxyglucose ($C_6H_{11}FO_5$)

Enters the biological processes instead of the glucose.
The radioisotope F-18 contained into the molecules decays emitting a β^+ with a ≈ 110 min lifetime.

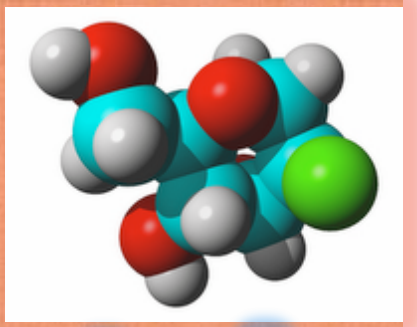

- ^{11}C-methionine ($C_5H_{11}NO_2S$)

Enters the processes linked to the protein metabolism. It is used also for the study of neural processes. (≈ 20 min lifetime)

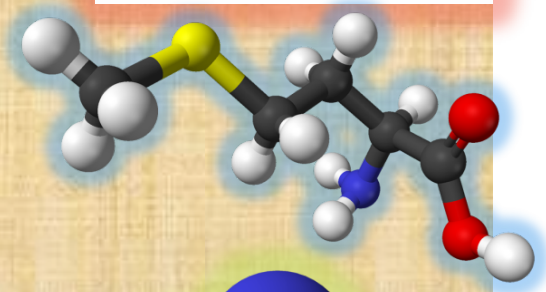

- ^{13}N-ammonia (NH_3)

Used for blood flux and miocardic tissue studies (≈ 10 min lifetime)

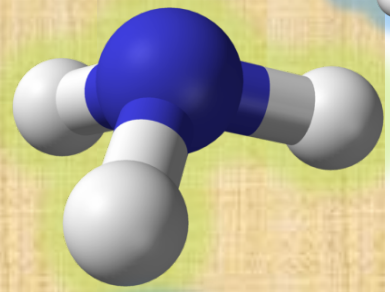

- ^{15}O-water (H_20)

Used for blood flux and muscles fibers functioning studies
(≈ 2 min lifetime.)

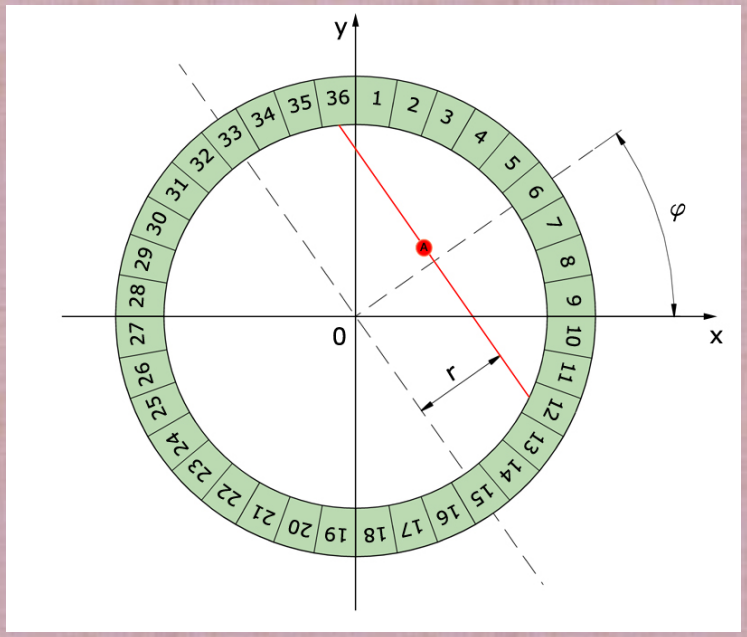

Key terms

- Line of response (LOR)
- Field of view (FOV)
- Sensitivity (χ)
- Time of flight (TOF)

$$\chi = \frac{\Omega}{4\pi} \cdot \phi \cdot \varepsilon_{pair} = \frac{cps}{activity}$$

Ω = solid angle coverage

Φ = packing factor

ε_{pair} = coincidence detection efficiency

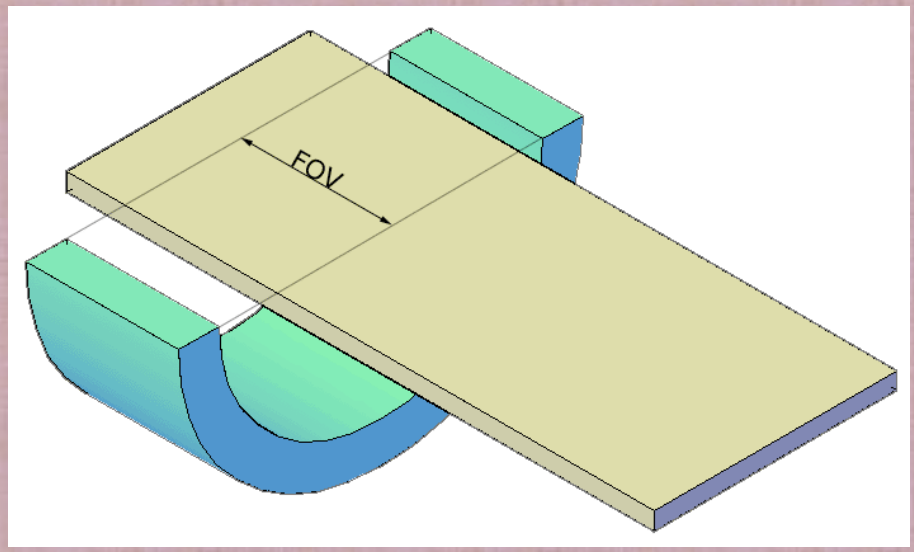

Detectors

Five main characteristics for a PET detector:

1) ***Reasonable high Stopping Power for 511 keV gammas***

   the higher the stopping power (dE/dx)(i.e. the lower the attenuation length), the thinner the detector (i.e. more compact) and the higher the efficiency

2) ***Signal decay time as short as possible***

   the shorter the decay time, the higher the rate capability and the lower the detector dead time

3) ***Light output (optic photons/keV released energy)***

   the higher the light output , the higher the energy resolution

4) ***Good Intrinsic Energy Resolution***

   the better the energy resolution, the higher the background rejection

5) ***Time of Flight capability***

   the better the time resolution , the higher the background rejection and the higher the SNR (Signal to Noise Ratio)

Inorganic Scintillating Crystals

Property	NaI(Tl)	BaF_2	BGO	CsF	CsI(Na)	GSO	$LaBr_3$	LYSO	LSO	YSO
Density ρ (g/cm^3)	3.67	4.89	7.13	4.61	4.51	6.71	5.06	7.4	7.4	4.53
Effective Z	50.6	52.2	74.2	53	54	58.6	46.9	66	65.5	34.2
Attenuation length (cm)	2.88	2.20	1.05	2.56	2.43	1.43	2.20	1.10	1.16	2.58
Decay constant (ns)	230	0.6	300	5	630	60	16	42	40	70
Light output (photons/keV)	38	2	6	1.4	28	10	56	11	29	46
Relative light out (%)	100	5	15	3.7	75	25	147	28.5	75	118
Wavelength (nm)	410	220	480	390	420	440	380	428	420	420
$\Delta E/E$ (%)	6.6	11.4	10.2	20	15	8.5	2.8	20	10	12.5
Index of refraction	1.85	1.56	2.15	1.48	1.84	1.91	1.86	1.82	1.82	1.8
μ (cm^{-1})	0.341	0.455	0.950	0.390	0.411	0.698	0.455	0.909	0.866	0.388
μ/ρ (cm^2/g)	0.095	0.093	0.133	0.084	0.091	0.104	0.0900	0.123	0.117	0.853
Hygroscopic	yes	no	no	yes	yes	no	yes	no	no	no

Main features for some of the most adopted scintillating crystals.

Signals from detectors

Usually crystals are optically coupled to photomultipliers

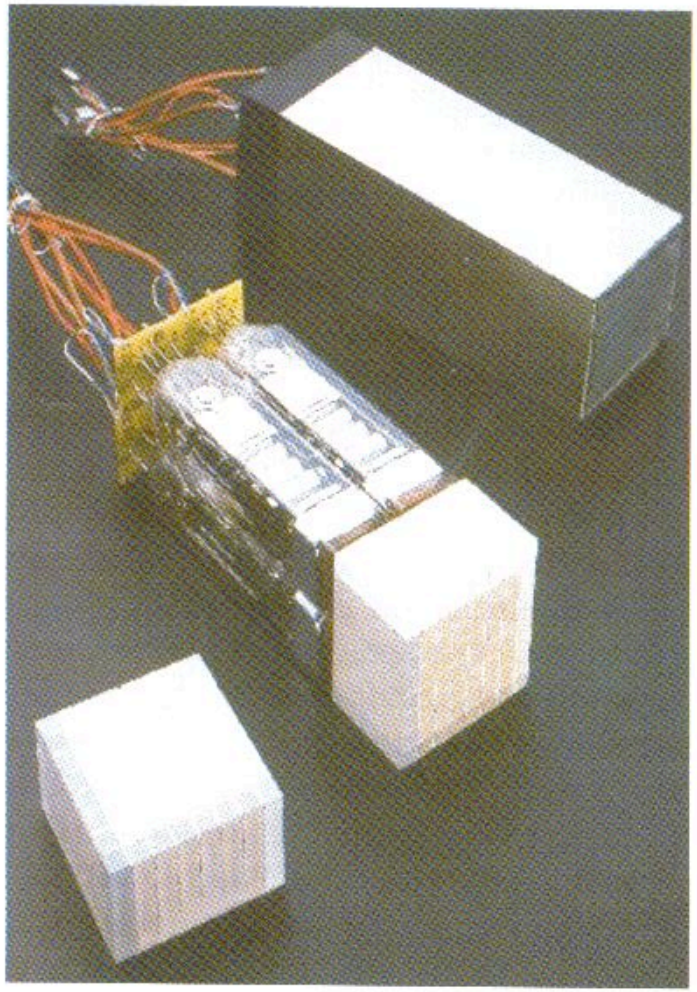

Figure 2.21. A block detector from a Siemens-CTI ECAT 951 PET scanner is shown. The sectioned (8 × 8 elements) block of BGO is in the bottom left corner, with the four square PMTs attached in the center, and the final packaged module in the top right corner. The scanner would contain 128 such modules in total, or 8192 individual detector elements. (Figure courtesy of Dr Ron Nutt, CTI PET Systems, Knoxville, TN, USA).

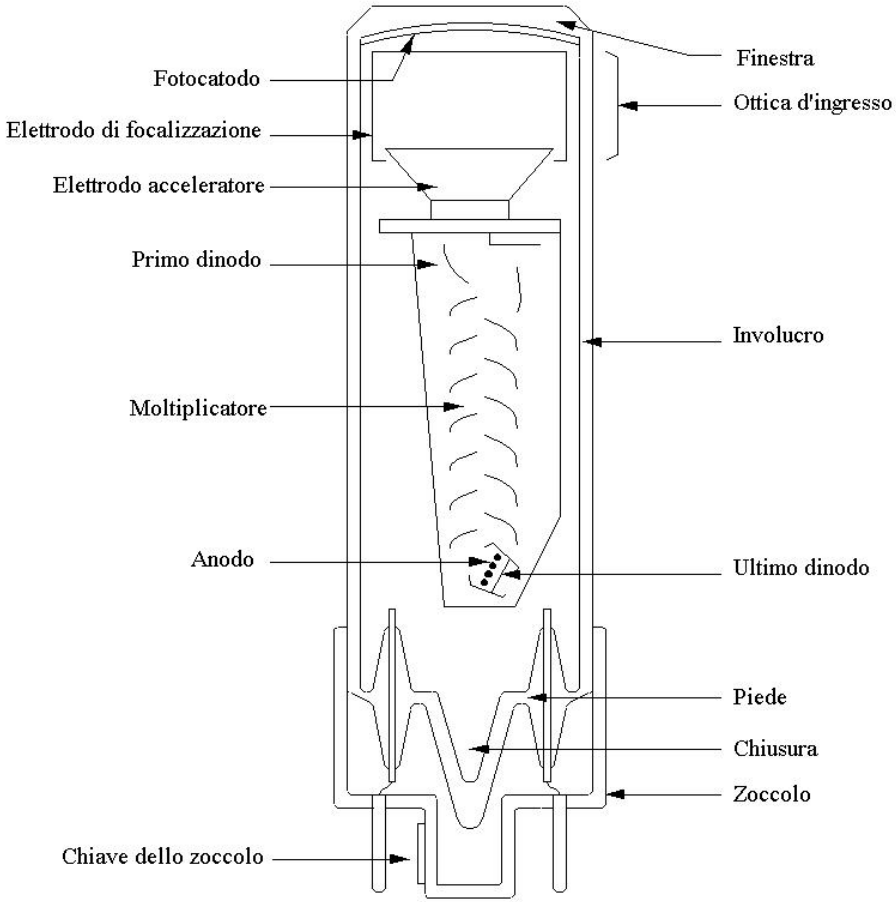

BGO Signal from a PMT.
The tail has been fitted with an axponential with 235.4 ns decay costant

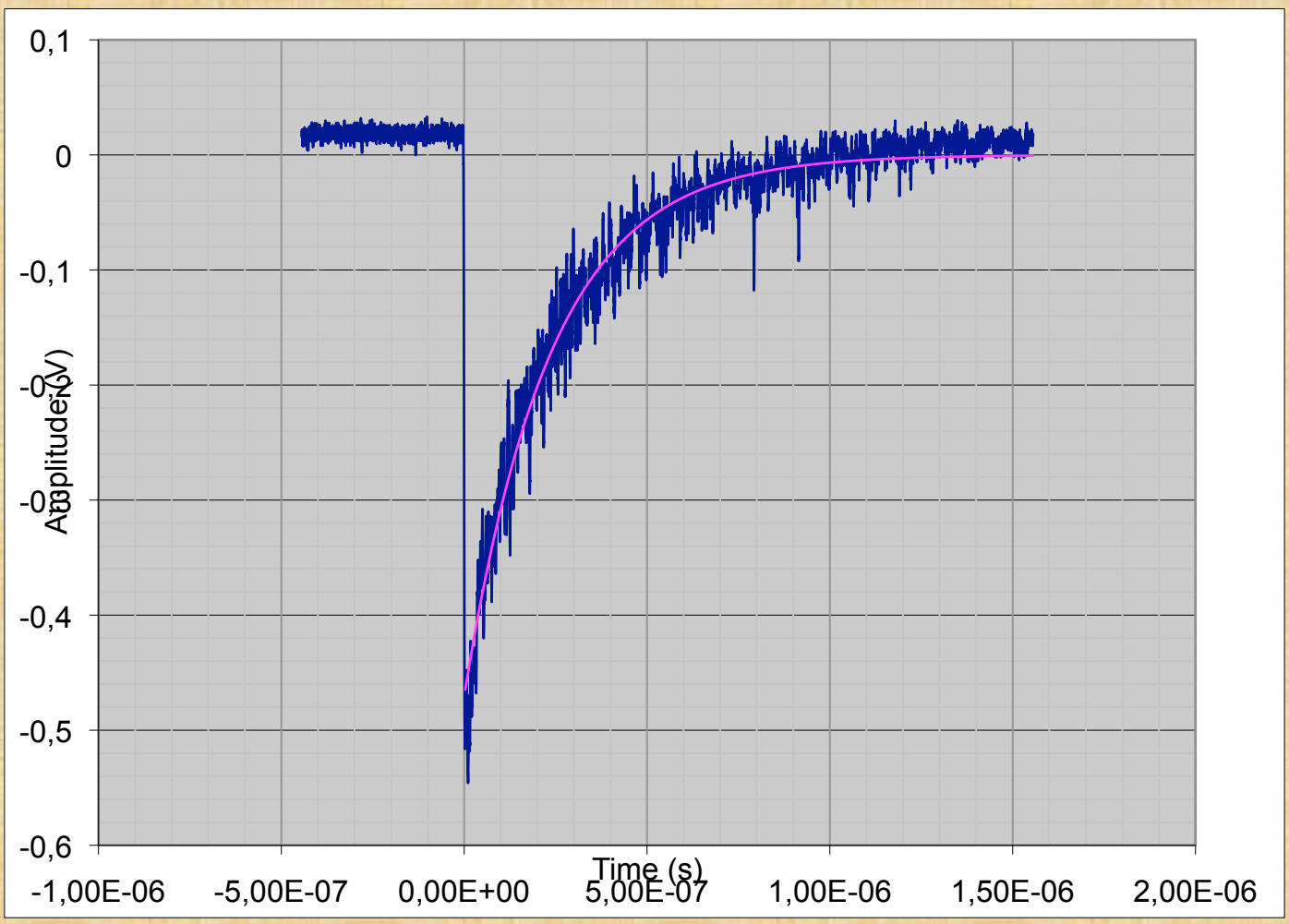

Error and noise sources

- Multiple hit
- Random coincidences
- Scattered coincidences

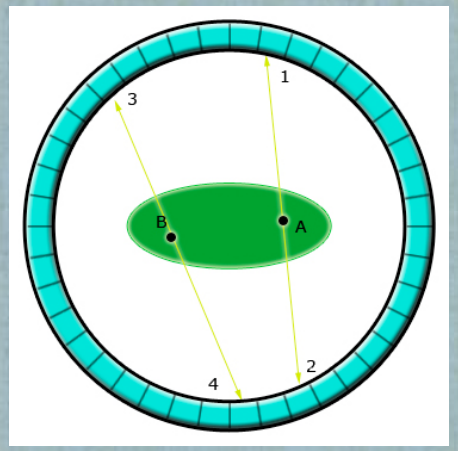

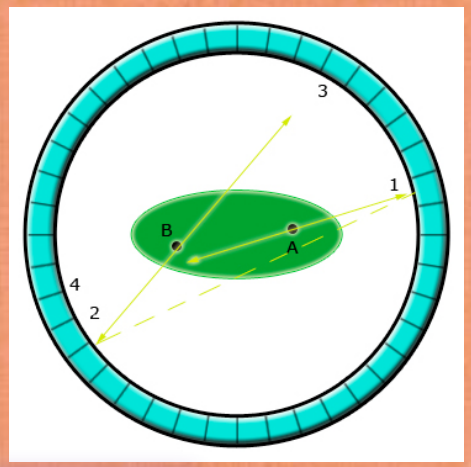

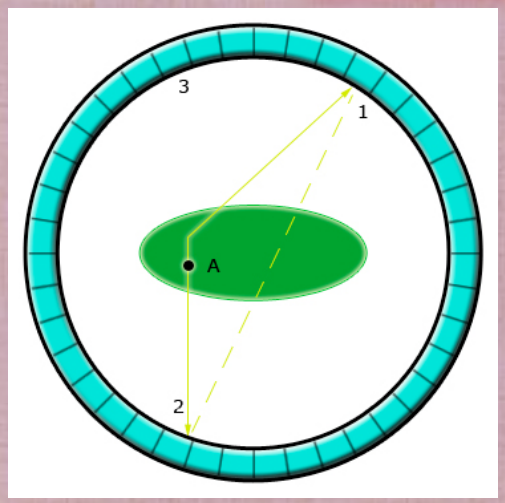

Scattered events are reduced by operating energy cuts (typically below 350 keV) and correcting data for attenuation.

$$R_{1,2} = 2 \cdot \tau \cdot r_1 \cdot r_2$$

Relative weight of rates : True, Randoms , Scattered, Multiples, NEC.

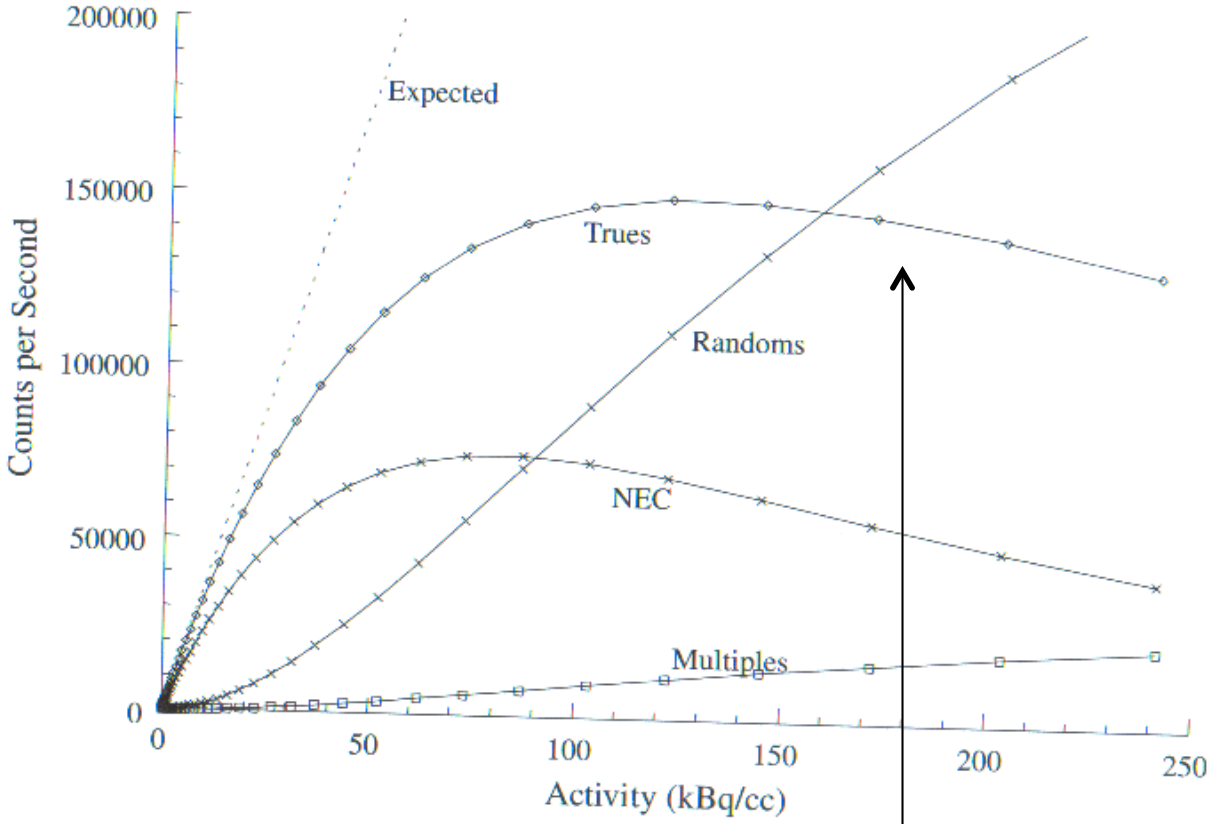

Figure 3.19. Count rate curves are shown for the measured parameters of true (unscattered plus scattered) coincidences, random coincidences, and multiple coincidences (three events within the time window), and the derived curves for expected (no counting losses) and noise equivalent count rate (NEC). The data were recorded on a CTI ECAT 953B PET camera using a 20 cm-diameter water-filled cylinder filled with ^{11}C in water.

Noise Equivalent Count Rate is a quality control parameter; it allows direct comparison among different scanners types.

$$N.E.C. = \left(\frac{T}{T+R+S}\right) \times T$$

Due to detector dead-time

[Tow]

Error and noise sources

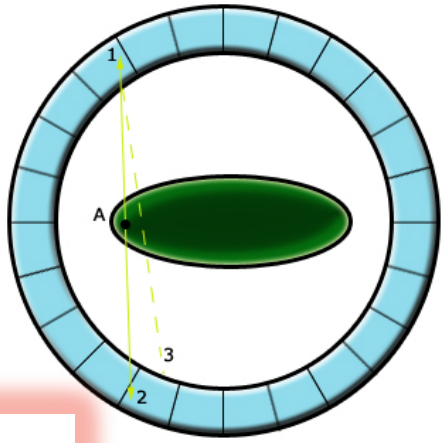

- Depth of interaction (DOI)
- Positron range
- Photons emission angle
  (FWHM= 0.5 degrees)

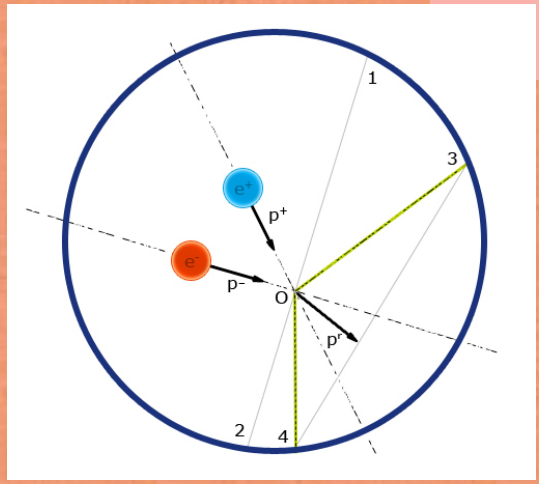

In water:

-50 % of events outside a 0.1 mm

-16 % of events outside a 0.25 mm radius

-9 % of events outside a 0.5 mm radius

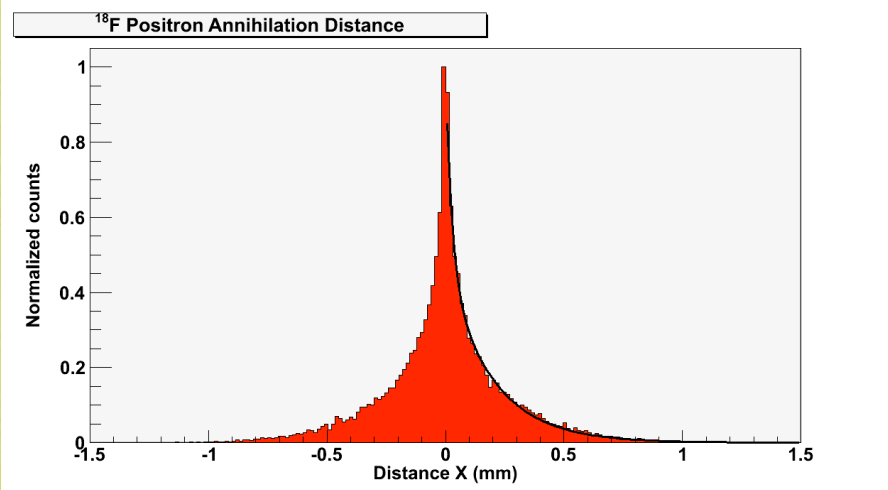

Sensitivity, FOV and Time Of Flight

- Sensitivity χ depends over-linearly on the FOV up to about 60 cm.
- Using TOF information leads to an increase of the S/N ratio.

$$\chi = \frac{\Omega}{4\pi} \cdot \phi \cdot \varepsilon_{pair}^{win}$$

$$S/N_{gain} \propto \sqrt{\chi} = \frac{2 \cdot d}{c \cdot \Delta t}$$

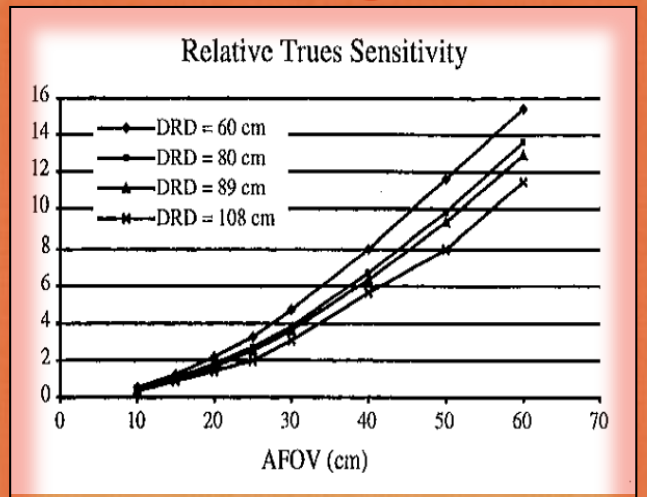

Total true coincidence for 1 hour whole body simulation as a function of FOV (plotted relative to a standard detector geometry) [Bad].

DRD= detector ring diameter

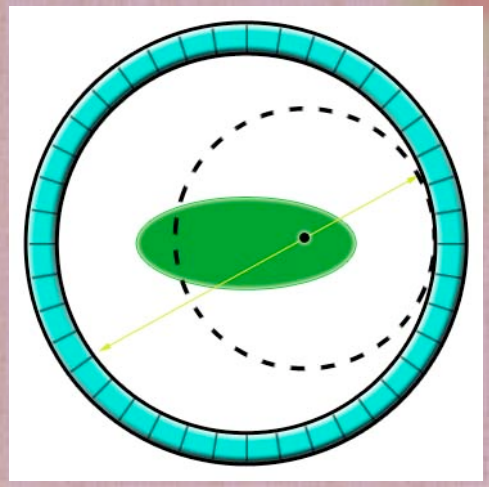

....more in detail...

- *In a PET exam about 10-13 mCi FDG are injected = 10 x 10^{-3} x 3.7 10^{10} Bq ≈ 3.7 x 10^{8} Bq = 370 MBq*
- *^{18}F has a half-life $\tau_{1/2}$ = 109 m = 6540 s*

1. *Let's calculate* $\lambda = \frac{\ln 2}{\tau_{1/2}} = \frac{0.693}{6540} = 1.06 \times 10^{-4} s^{-1}$ *(we need this afterwards)*

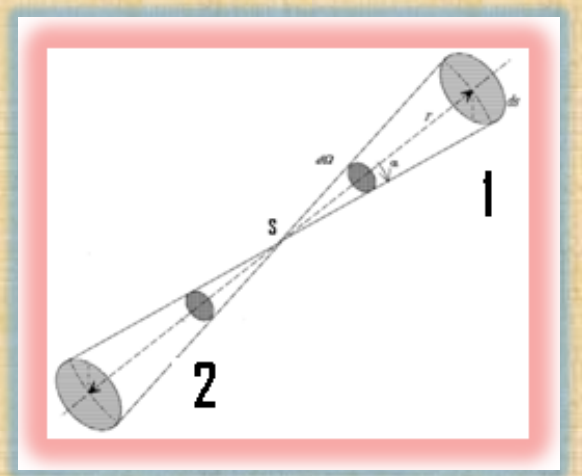

Consider the coincidence detection of two gammas emitted back to back from a source located at the center wrt two opposite detectors.

$$\varepsilon_1 = \frac{R_c}{R_2} \quad R_c = \varepsilon_1 (A \frac{d\Omega}{4\pi} \varepsilon_2) \quad \text{if } \varepsilon_1 = \varepsilon_2$$

$$R_c = A \frac{d\Omega}{4\pi} \varepsilon^2$$

$$\frac{R_c}{A} = \frac{d\Omega}{4\pi} \varepsilon_{pair}^{win} = \chi$$

Coincidence system

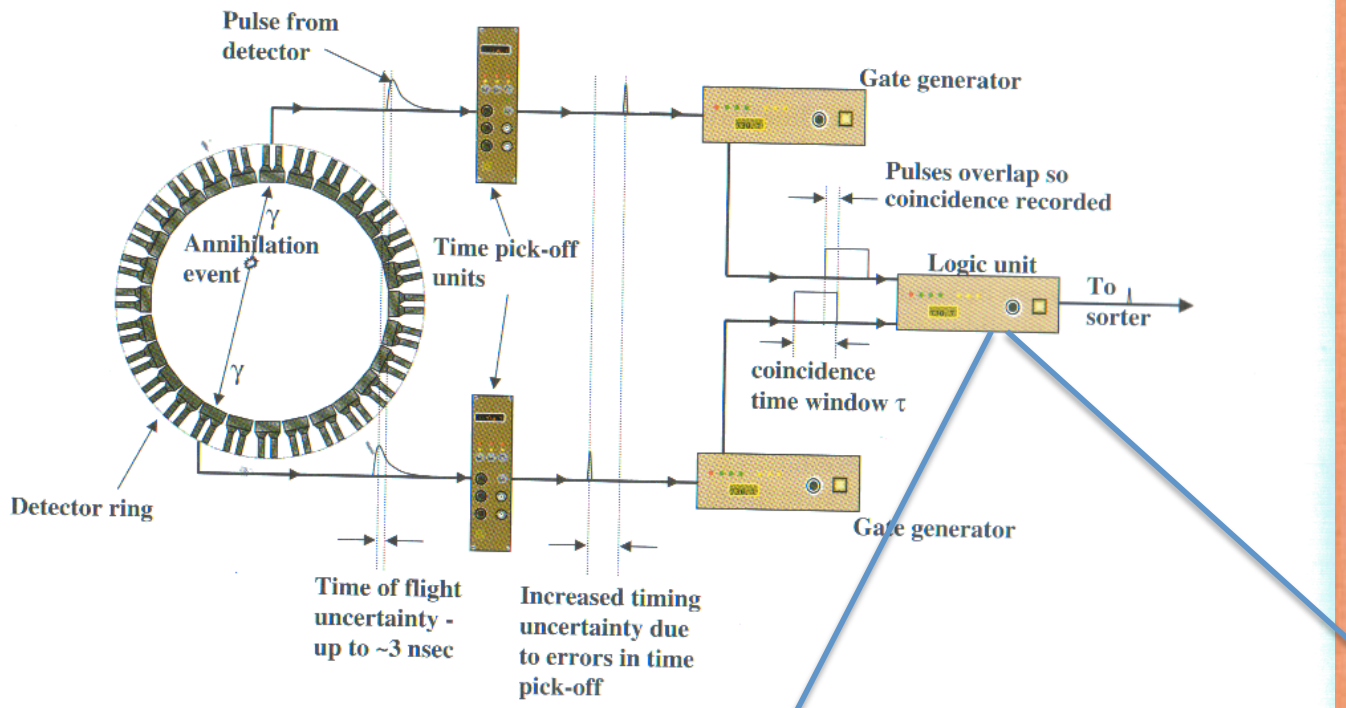

- *Time arrival definition (time pick-off)*
- *Time window definition (gate generator)*
- *Coincidence Logic (logic unit)*

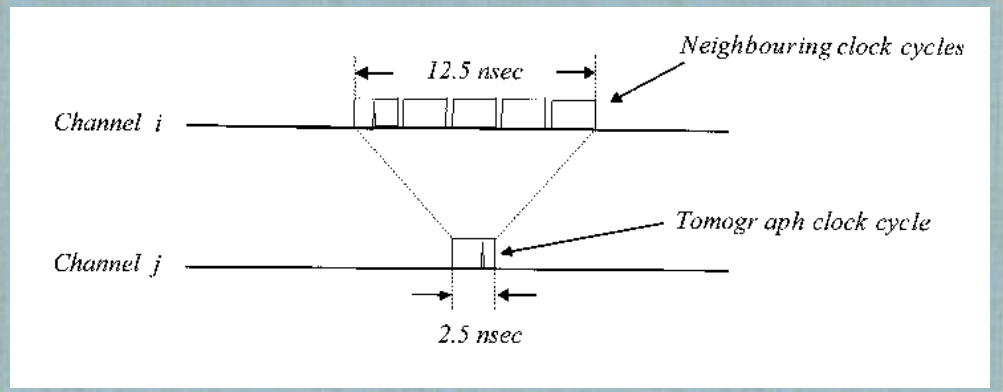

2. How to calculate the spurious coincidences ?

If R1 and R2 are the detector's count rates (s^{-1}) and 2τ the coincidence time window the random coincidence count rate is $F = 2\tau R_1 R_2$

$2\tau R_1 \longrightarrow$ *Number of counts from detector 1 when detector 2 opens the time window*

Q: how frequent the time window is opened ? $\longrightarrow$ R_2

A consequence of this formula is that the smaller the coincidence time window, the smaller the random coincidences contribution (hence the smaller the reconstructed image background)

→ ***Fast detectors are required***

Let's calculate the probability of having at least 2 contemporary decays

$$P(k,\mu) = \frac{\mu^k}{k!} e^{-\mu} \quad , \quad \mu = \lambda N \Delta t$$

$$\lambda = \frac{1}{\tau} \qquad \lambda N = 370\ \text{MBq}$$

Δt is can be thougth to be the signal formation time or the coincidence time window

$$\mu = \lambda N \Delta t = 370 \times 10^6 \times 10^{-8} = 3.7$$

$$P(0,\mu) = e^{-\mu} = 0.025 = 2.5\%$$

Δt = 10 ns

$$P(1,\mu) = \frac{\mu^k}{k!} e^{-\mu} = 3.7 e^{-3.7} = 0.091 = 9.1\%$$

So the probability to have at least 2 decays is:

$$P(\geq 2,\mu) = 1 - P(0,\mu) - P(1,\mu) = 100\% - 2.5\% - 9.1\% = 88.4\%\ !!$$

So for sure in a PET exam we have to take into account multiple decays....

Among all this multiple decays which are those unwanted ?

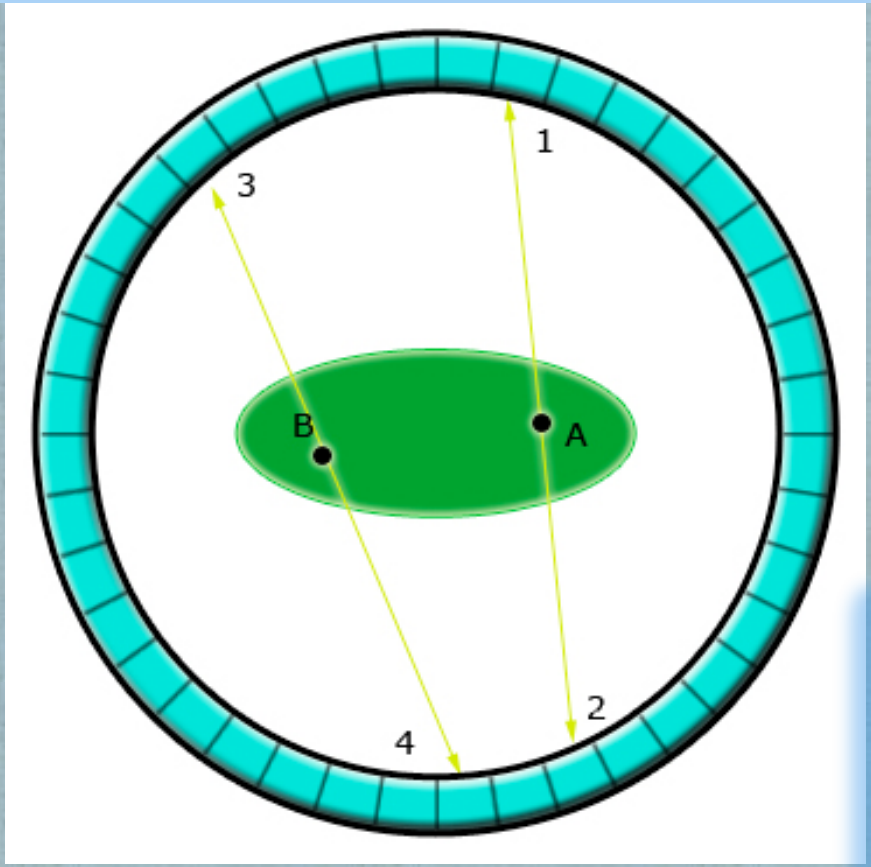

OK !

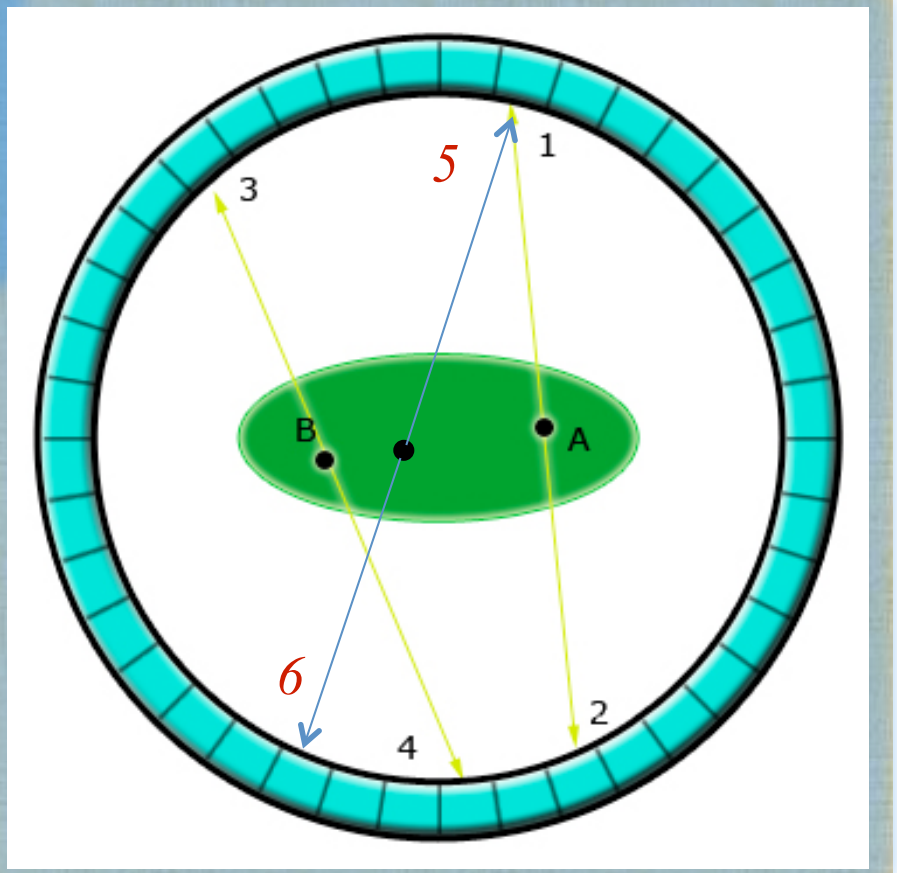

KO !

The counts in a detectors represent the line integral of the decays along the LOR so in this case event # 5 is noise for LOR(1-2) ...

Some numbers:

The PET exam (i.e. the real measurement) takes some 15'-30' (FDG :according to the different targets. For ^{11}C –colina: 30'-60') but some time after the injection is spent for distribution into the tissue and uptakes into the organs (+ 1h)

FDG 5.18 MBq/kg (2 min/position x 6-9 positions in a PET total body)

$$A(\Delta t) = A(0)e^{-\lambda \Delta t}$$

$$A(1h) = A(0)e^{-1.06\times10^{-4}\times3.6\times10^{3}} = A(0)e^{-0.382}$$

$$\frac{A(1h)}{A(0)} = 68.3\%$$

Only 68% of the injected activity is used for the PET measurements

(Dose is on average 7 mSv for a PET scan)

Image Reconstruction

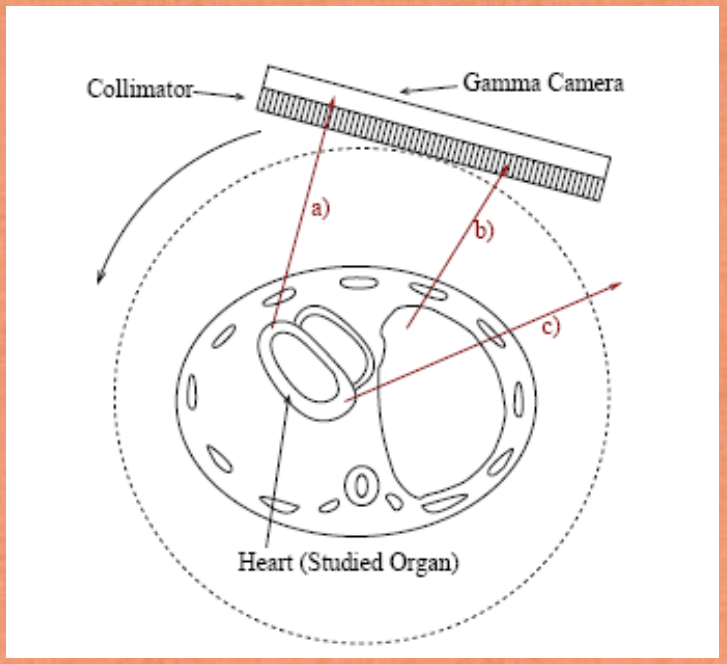

The image generated on the detectors for each projection represents the Radon Tansform of the object so the problem is how to inverse the Radon Transform.

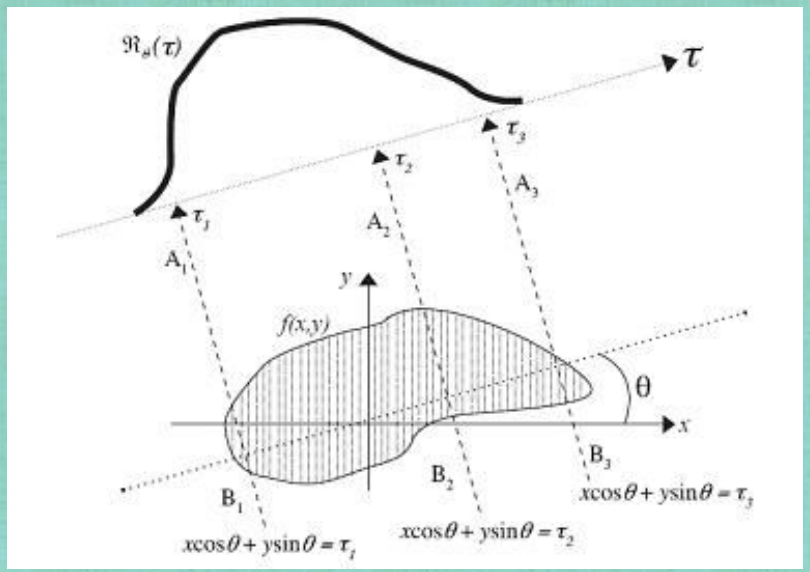

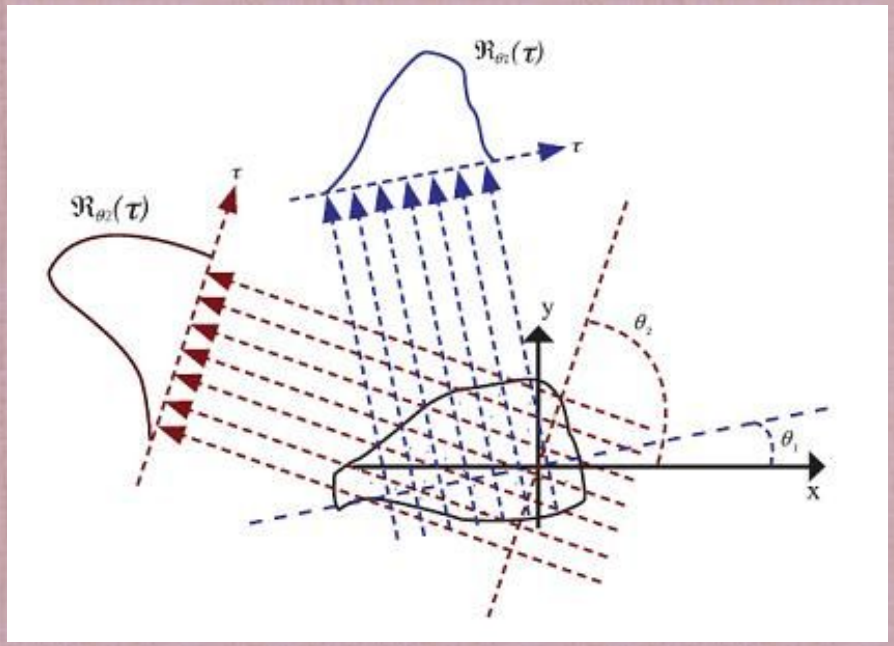

Image Reconstruction

Iterative algorithms like Expectation Maximization (EM) based on iterative:

1. *Projection (an estimate of each voxel intensity is "projected" on each pixel)*
2. *Correction Image (real content of each pixel is normalized to the projection estimate)*
3. *Backprojection (the normalized value is used to backproject to the voxel)*
4. *Update (the voxel intensity estimate is updated)*

$$\nu_j^{k+1} = \nu_j^k \frac{\sum_{i=1}^{I} \frac{p_i w_{ij}}{(\sum_{m=1}^{J} w_{im}\nu_m^k)}}{\sum_{i=1}^{I} w_{ij}}$$

I = Number of pixels (i indexed)

J = Number of voxels (j indexed)

w_{ij} = prob. of a photon emitted from voxel ν_j being recorded at detector p_i

1. $$\nu_j^{k+1} = \nu_j^k \frac{\sum_{i=1}^{I} \frac{p_i w_{ij}}{(1.)}}{\sum_{i=1}^{I} w_{ij}}$$

2. $$\nu_j^{k+1} = \nu_j^k \frac{\sum_{i=1}^{I} 2.w_{ij}}{\sum_{i=1}^{I} w_{ij}}$$

3. $$\nu_j^{k+1} = \nu_j^k \frac{3.}{\sum_{i=1}^{I} w_{ij}}$$

4. $$\nu_j^{k+1} = \nu_j^k 4.$$

[Chid]

TOF-PET detector requirement

- Good time resolution (< 3 ns for human PET)
- Good space resolution (< 1 mm)
- High efficiency
- Good energy resolution
- Affordable price per unit area
- Robustness
- Easy of operation

Resistive Plate Chambers

- RPC are gas detectors largely adopted in high energy physics.
- Charged particles ionize the gas producing ion-electron pairs; free electrons are accelerated by an external electric field and produce secondary ionization pairs.
- The resulting multiplicative effect leads to a charge avalanche which induces an electric signal on pick-up electrodes.

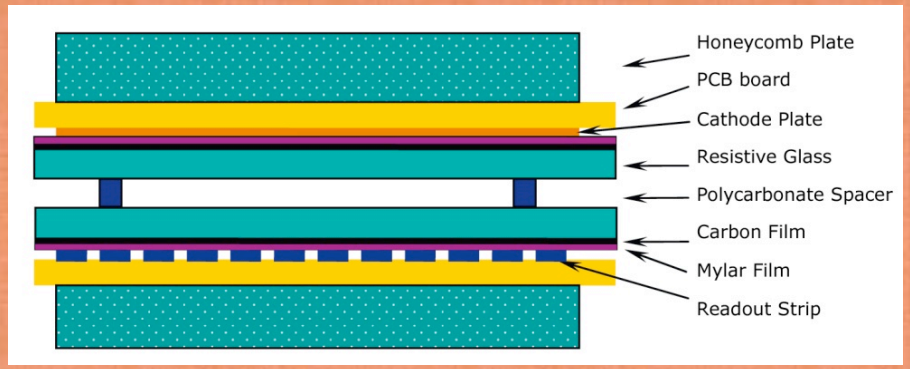

Standard RPC layout

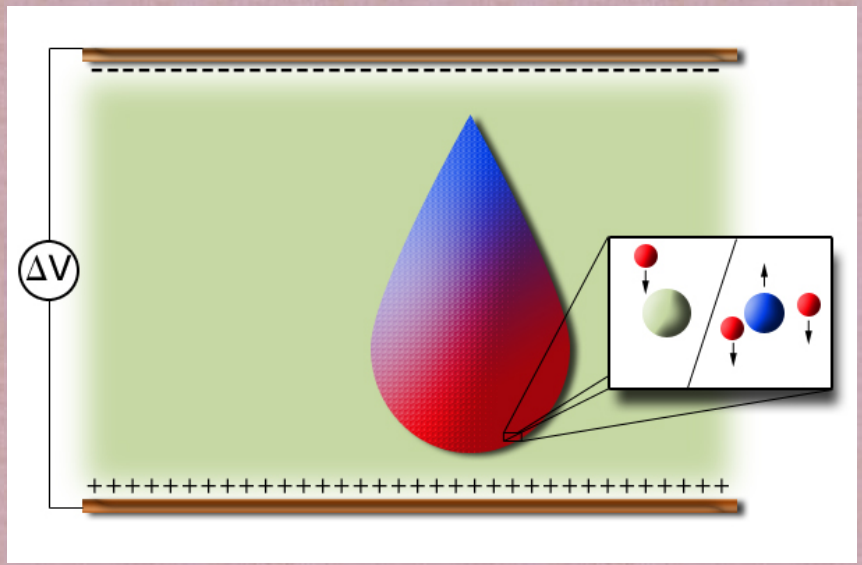

Avalanche development: gas molecules (green) are ionized producing electrons (red) and positive ions (blue).

RPC as gamma detectors

- In order to increase the gamma detection efficiency it is necessary to increase the interaction probability:
  - High Z plates
  - Increase the number of plates
- MultigapRPC configuration
  - Increase efficiency
  - Better time resolution
- Multi-stack configuration

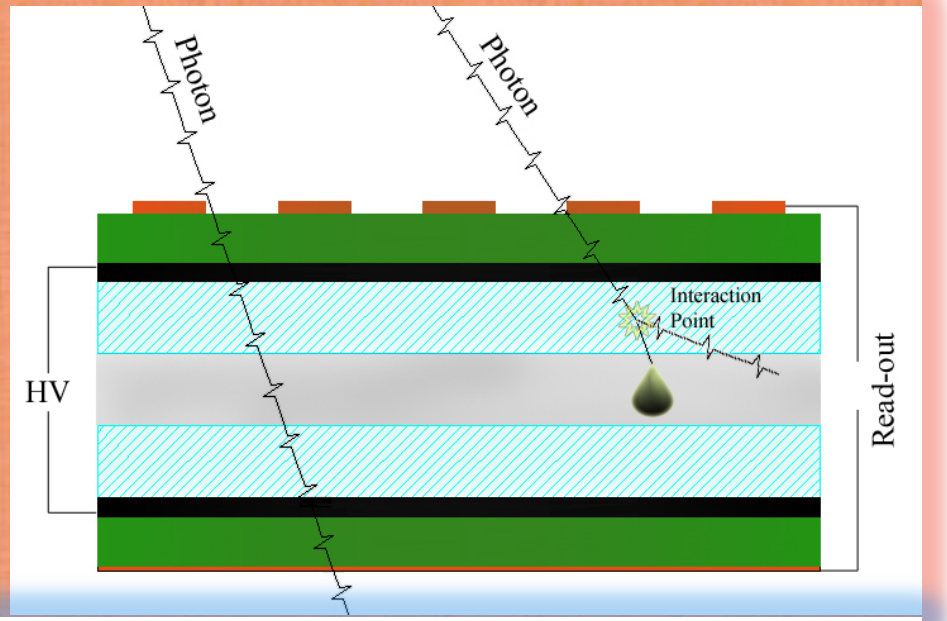

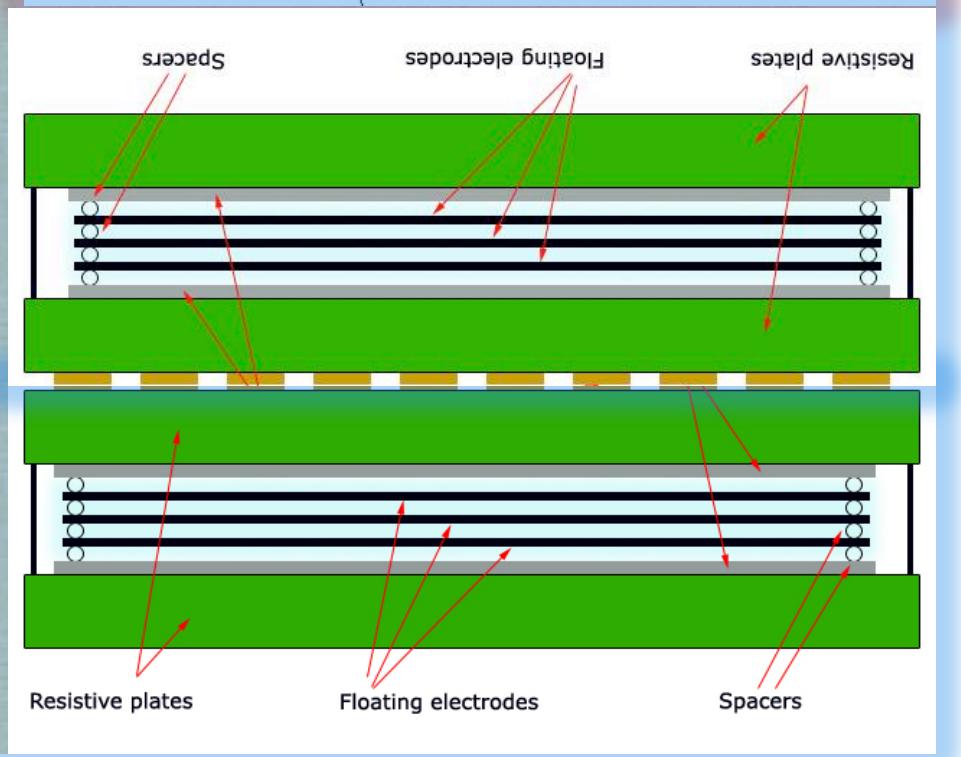

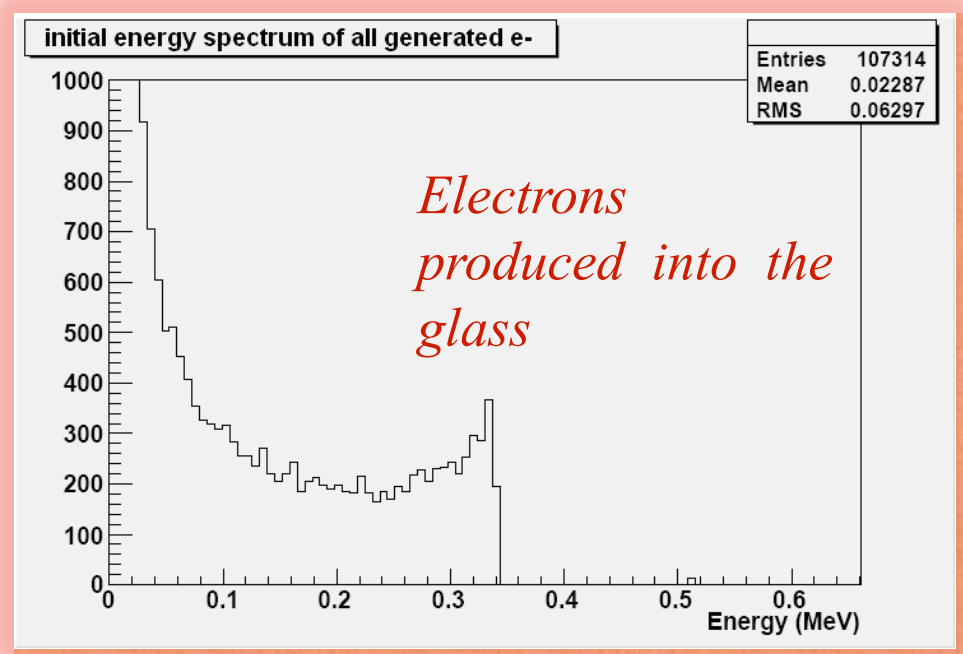
initial energy spectrum of all generated e-
Entries 107314
Mean 0.02287
RMS 0.06297
Electrons produced into the glass
Energy (MeV)

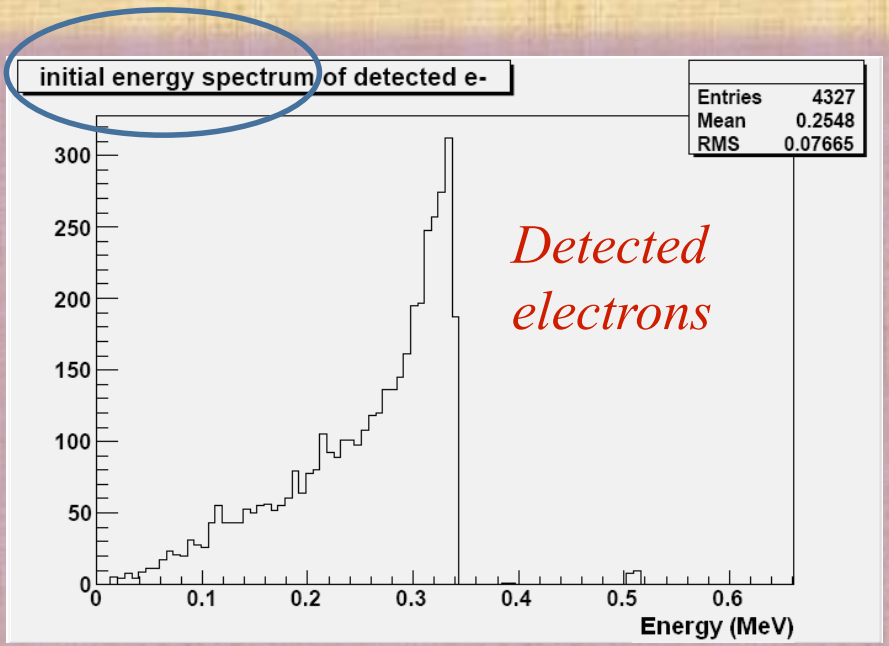
initial energy spectrum of detected e-
Entries 4327
Mean 0.2548
RMS 0.07665
Detected electrons
Energy (MeV)

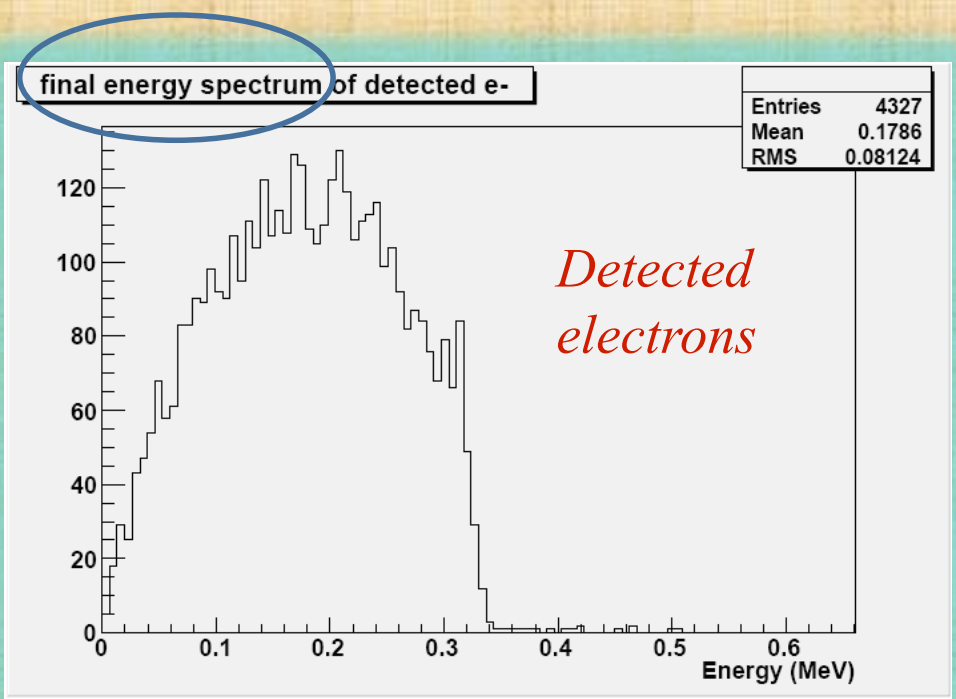
final energy spectrum of detected e-
Entries 4327
Mean 0.1786
RMS 0.08124
Detected electrons
Energy (MeV)

Efficiency vs. Glass thickness

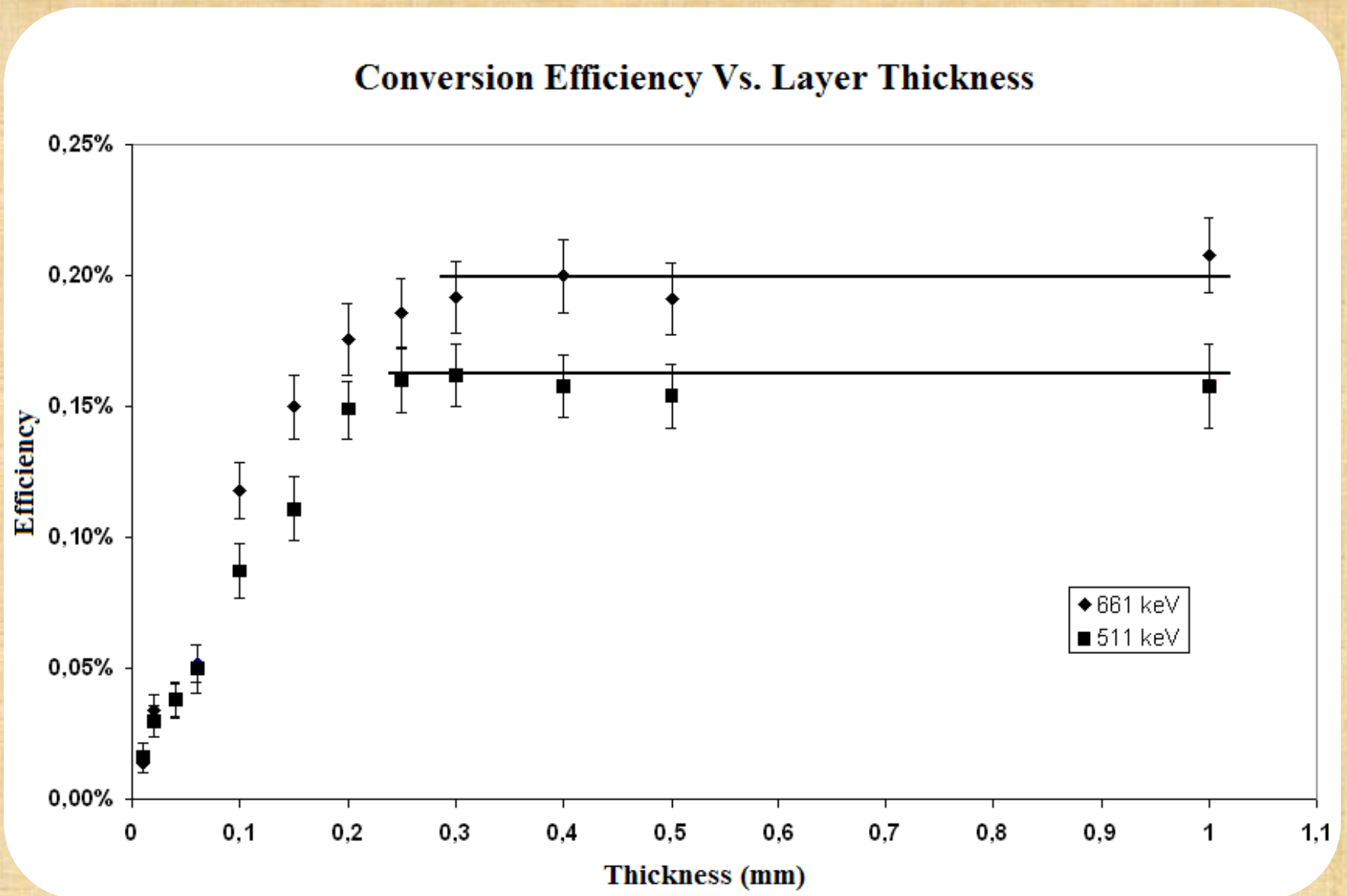

(Our) First Prototype for gamma efficiency measurements(2006)

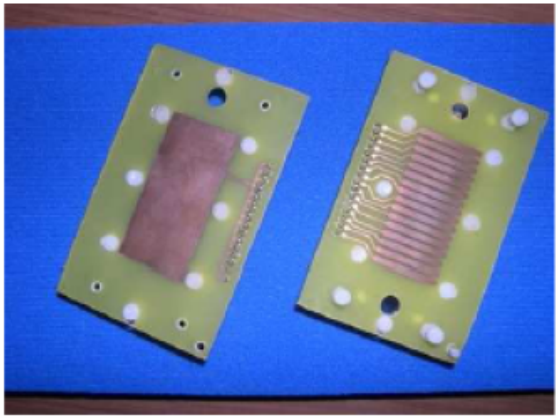

a)

b)

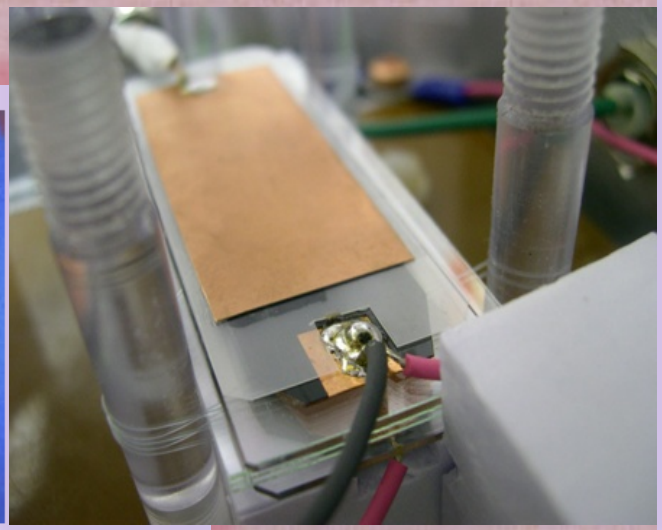

Fig.5 a) printed circuits boards were used as main MRPC structure on which copper strips or pads were engraved; b) standard microscope analysis glasses were used for the external electrodes; a semi conductive adhesive tape was used as HV and ground distribution.

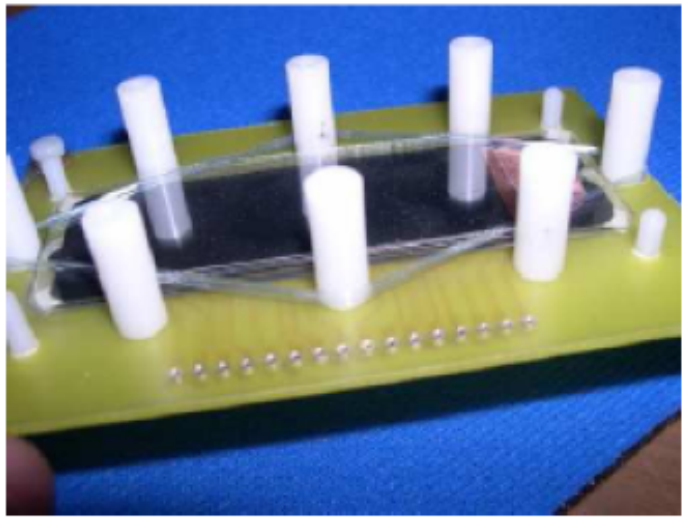

a)

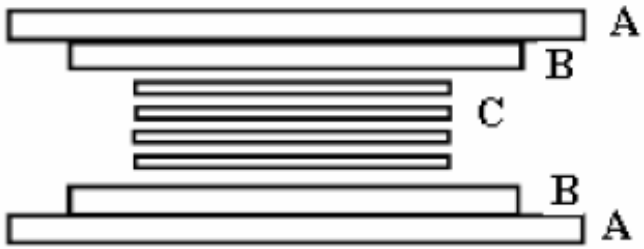

b)

Fig.6 a) Typical MRPC structure: teflon columns are inserted in the bottom printed circuit board to assure rigidity. The bottom HV electrode is visible as well as some gaps made with nylon fishing-line. In the foreground the holes allow

(Our) First Gamma Efficiency result (2006)

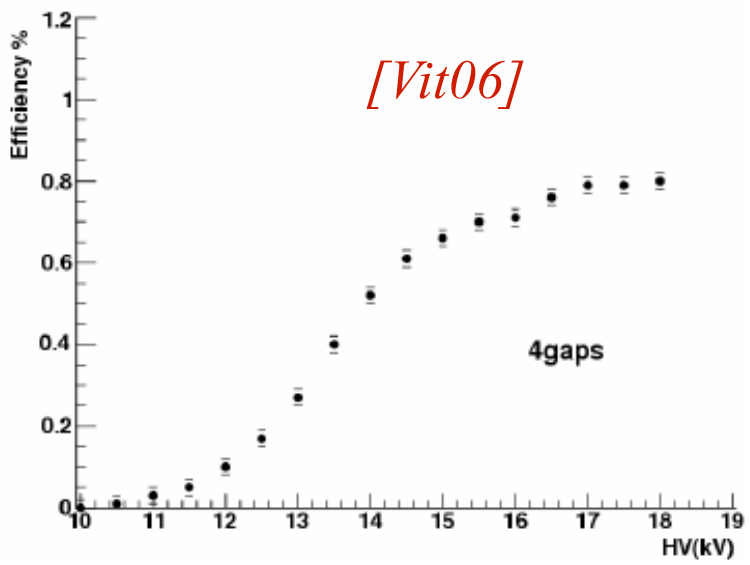

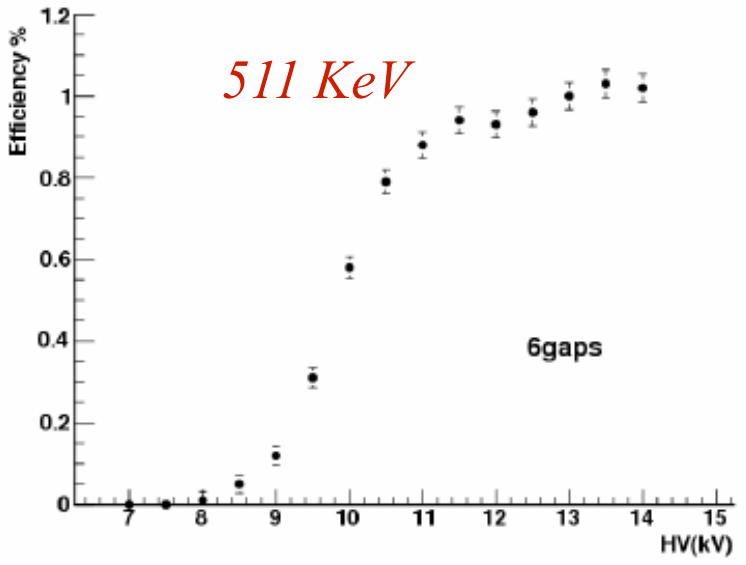

Fig.12. 511 keV gamma efficiency vs. applied HV for multigap RPCs for: a) 4 gaps RPC; b) 6 gaps RPC.

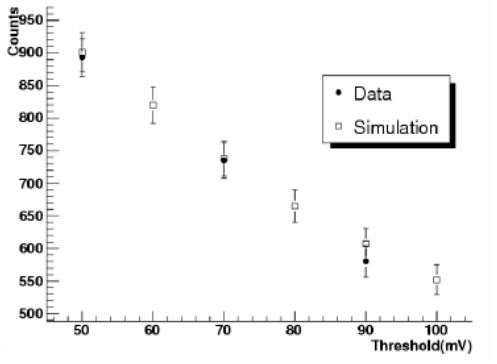

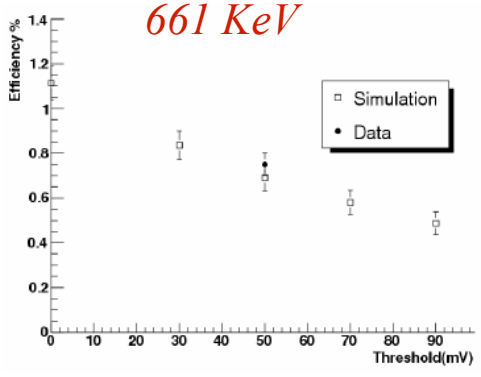

Fig.10. a) ^{137}Cs gamma counting vs applied threshold (x20); the simulated values have been normalised to the experimental ones (at 70 mV). The trend vs applied threshold seems to well reproduce the other experimental data; b) gamma efficiency (from ^{137}Cs) vs applied threshold for a 5 MGRPC. No normalisation of the simulated data has been applied.

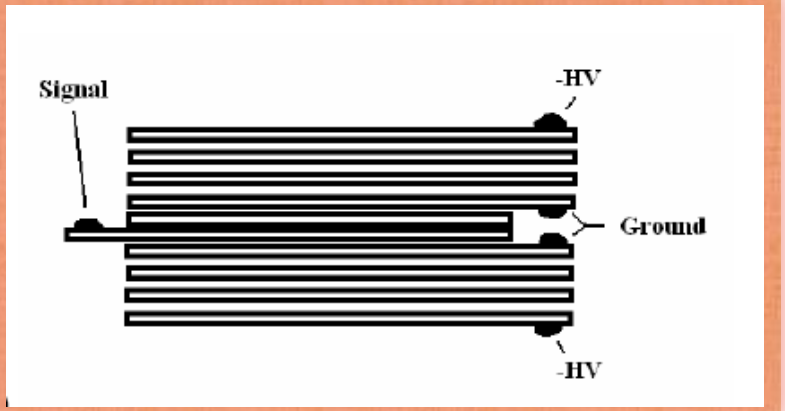

Gamma Efficiency vs. N. of gaps

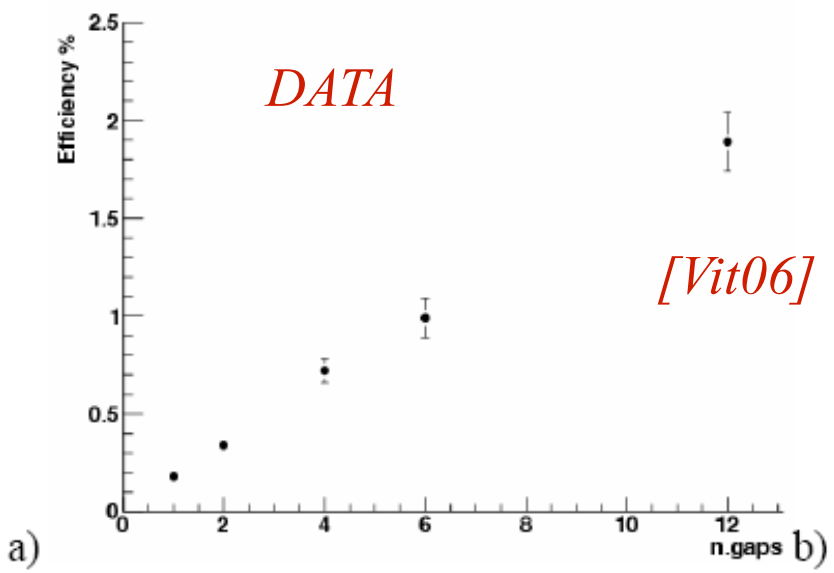

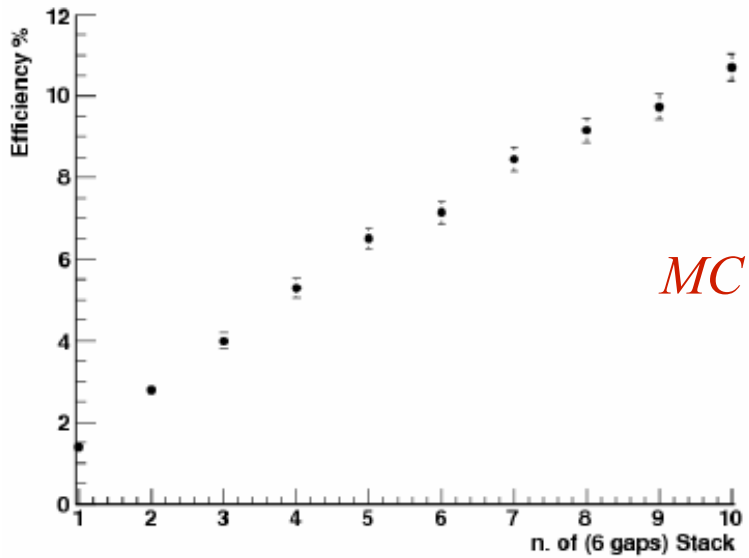

Fig.13 a) Experimental data: 511 keV gamma efficiency vs. number of gaps. Discrimination threshold set to 2.5 mV (1 to 6 gaps) and 5 mV (12 gaps); b) Geant4 simulation of 511 keV gamma efficiency vs. number of (6 gaps) stacks.

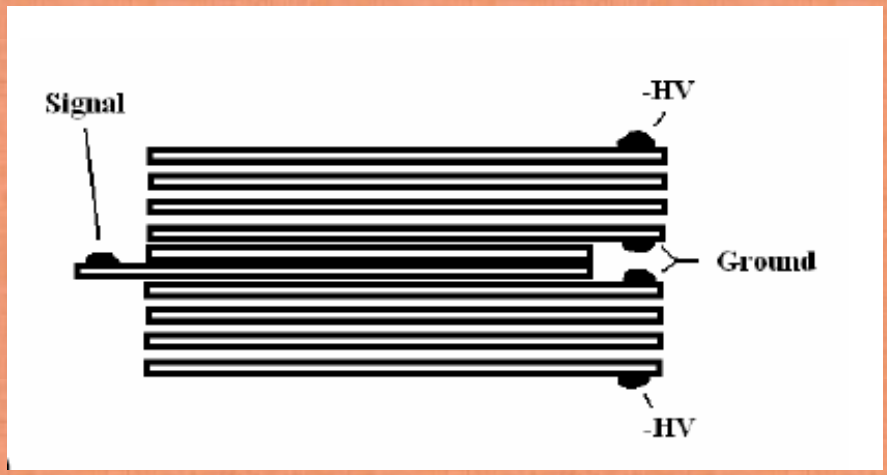

Gamma Efficiency vs. N. of gaps

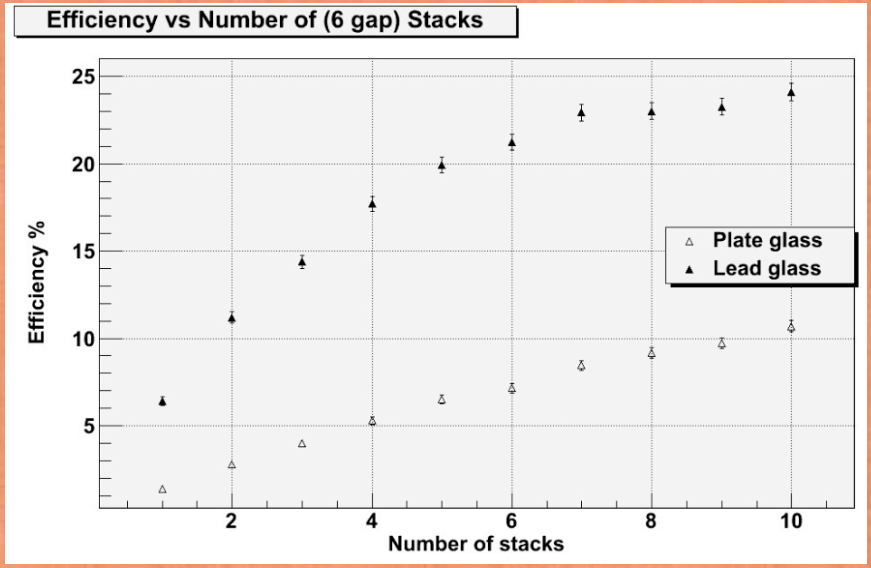

[Vit06]

MC

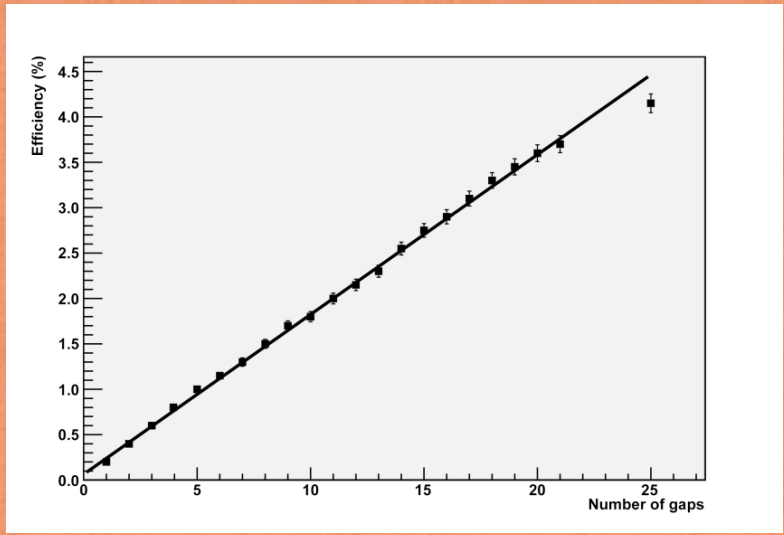

Efficiency of a stack of 0.4 mm glass plates for the detection of 511 keV photons as a function of the number of gaps.
The results from two independent studies are in good agreement (at least for few gaps).

MC + (1) Datum

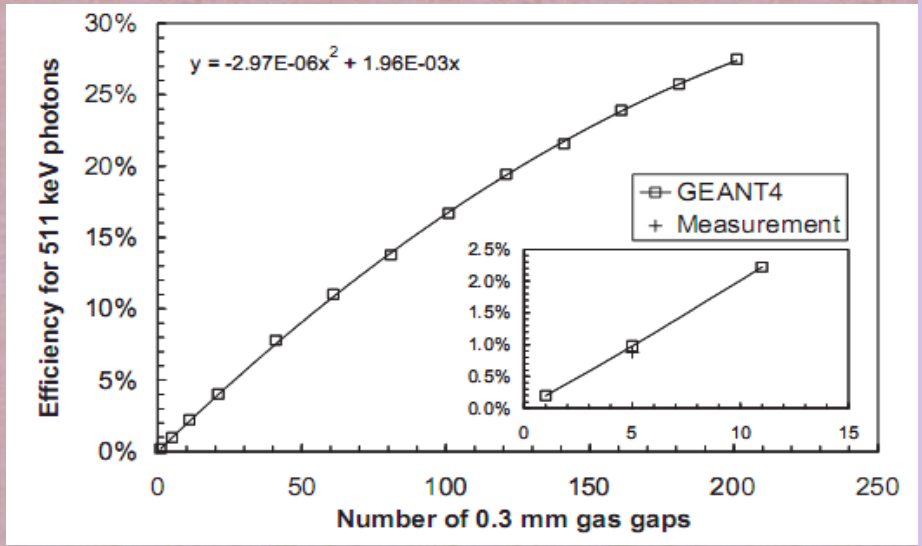

[Cou07]

Number of Gaps	Gamma efficiency (511 keV) @ 2.5 mV			E in the gap at the knee of the plateau
	GEANT4	Data	Error	
1	0.18%	0.18%	0.03%	10.6 kV/mm
2	0.29%	0.34%	0.03%	10.7 kV/mm
4	0.75%	0.72%	0.03%	11.3 kV/mm
6	1.17%	0.99%	0.06%	10.9 kV/mm
12	2.23%	1.89%*	0.06%	10.6 kV/mm

Tab.1 511 keV gamma efficiency vs. Number of gaps: the values correspond to the plateau region of the efficiency curves. Simulated values (calculated at 0 discrimination threshold) are reported on the second column; experimental data are shown in the third column as well as the associated errors (fourth column). The discrimination threshold was 2.5 mV. In the last column the value of the electric field in the gap at the knee of the plateau is calculated. * For the value corresponding to 12 gaps a discrimination threshold of 5 mV were selected.

[Vit06]

DATA

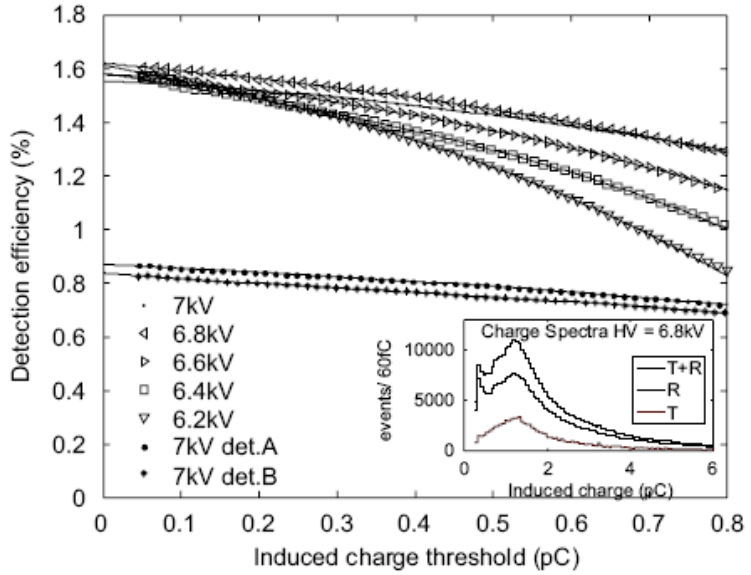

Fig. 6. Measured detection efficiency as a function of the threshold used for signal detection, converted to the charge induced on the electrodes. The interpolating cubic polynomial extrapolated to zero charge yields the intrinsic efficiency, which may be compared with the simulations. The inset shows an example of the corresponding charge distribution (see Fig. 5 for the definitions of T and R).

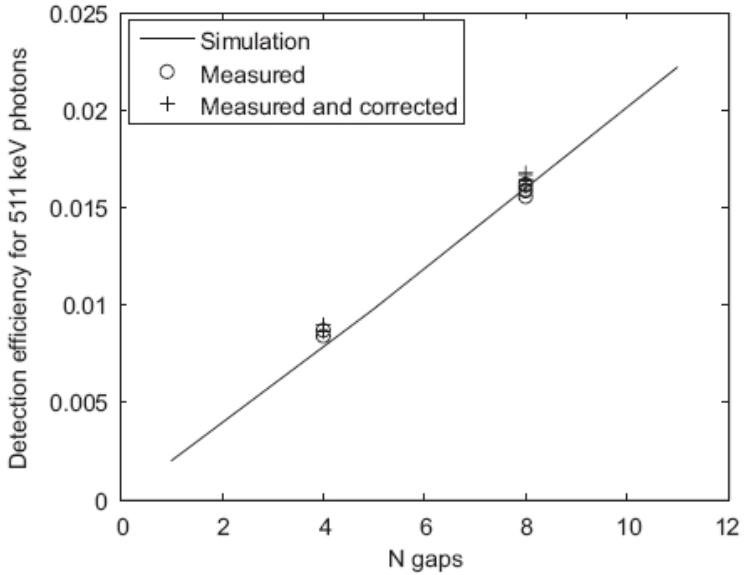

Fig. 7. Comparison between the measurements shown in Fig. 6 (all curves), the measurements corrected by the setup efficiency and the simulations, showing a very good agreement.

plates the optimum plate thickness ranges from 280 to 380 μm for

[Bla09]

Gamma Efficiency vs. photon energy - (MC)

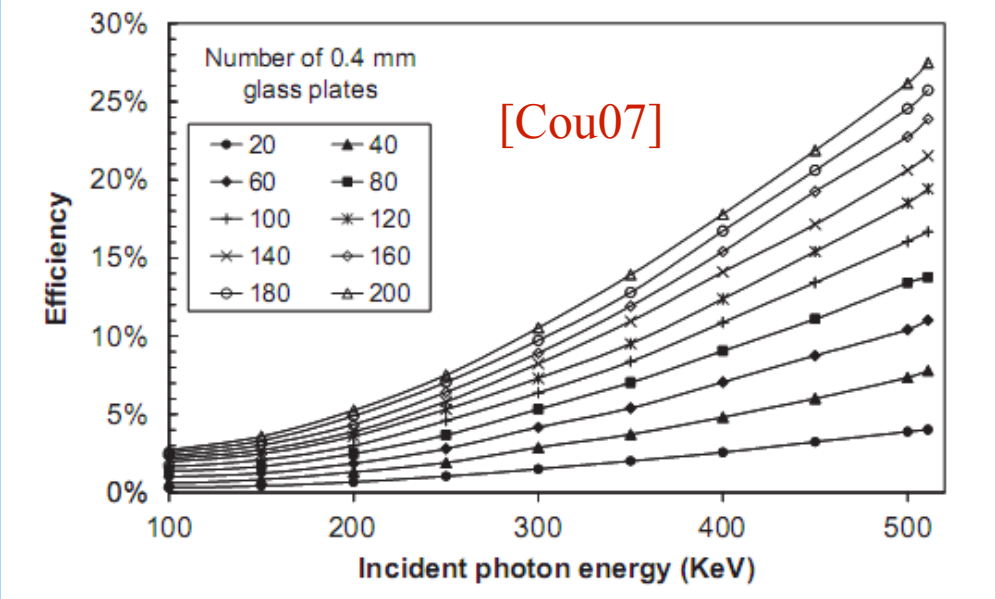

[Cou07]

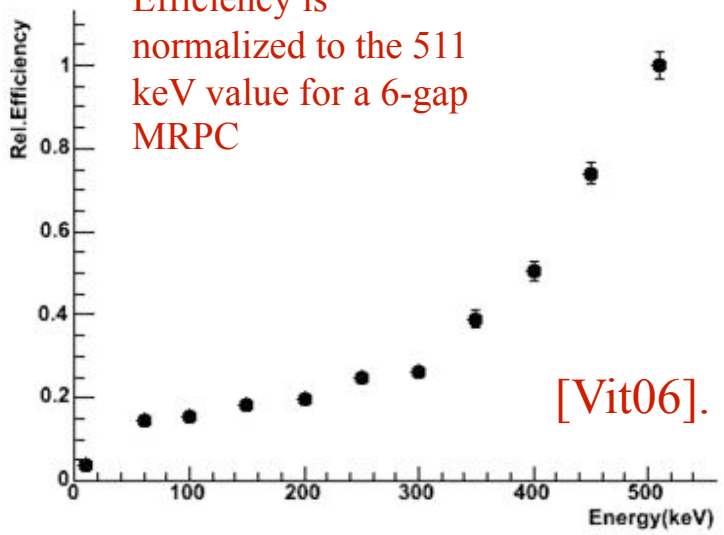

Efficiency is normalized to the 511 keV value for a 6-gap MRPC

[Vit06].

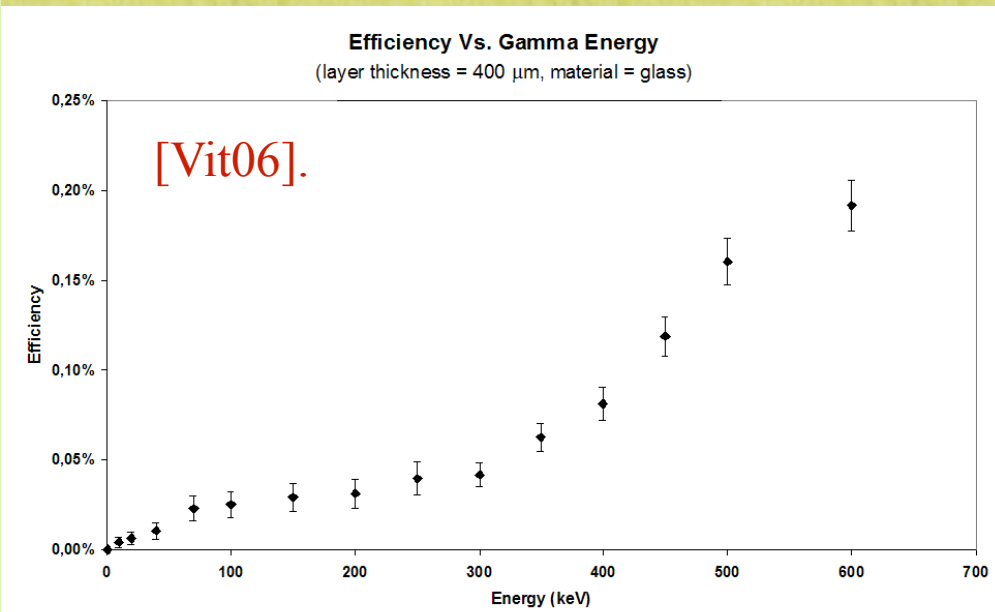

[Vit06].

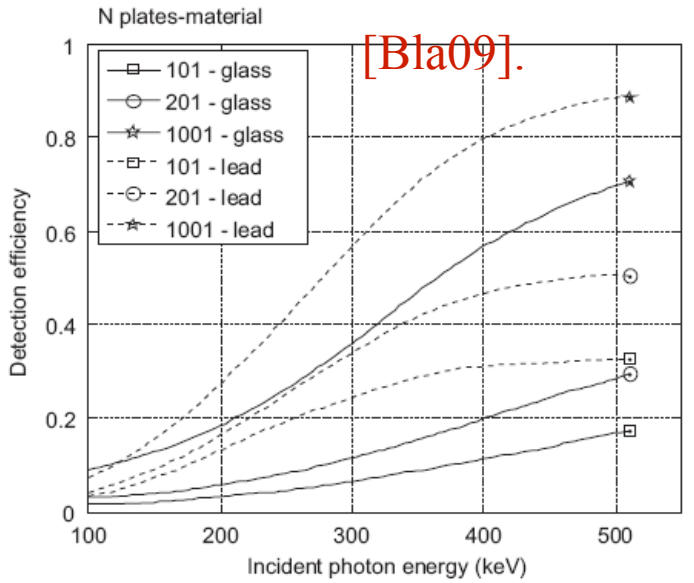

[Bla09].

Fig. 2. Detection efficiency as a function of the incident photon energy for stacks of glass and lead optimum-thickness plates. The curves for lead-glass (not shown) are very similar to those of lead.

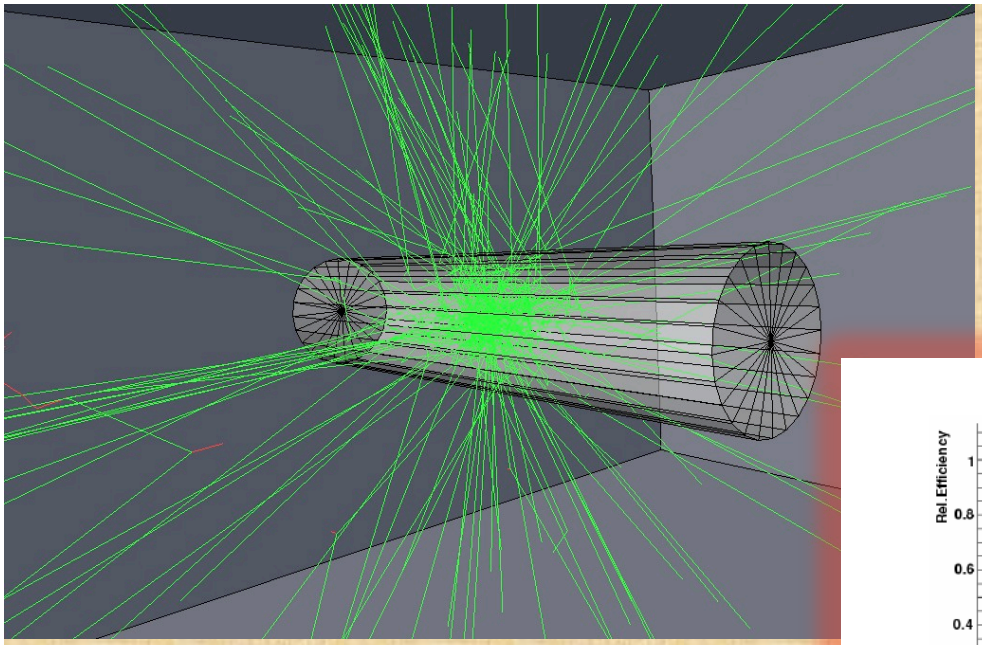

MGRPC Simulation: Peak to total area

How RPCs reduce the scatter fraction

[Vit06]

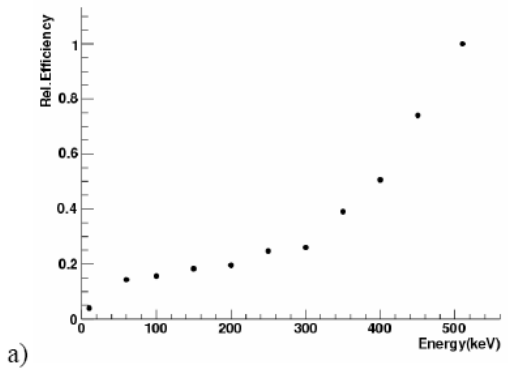

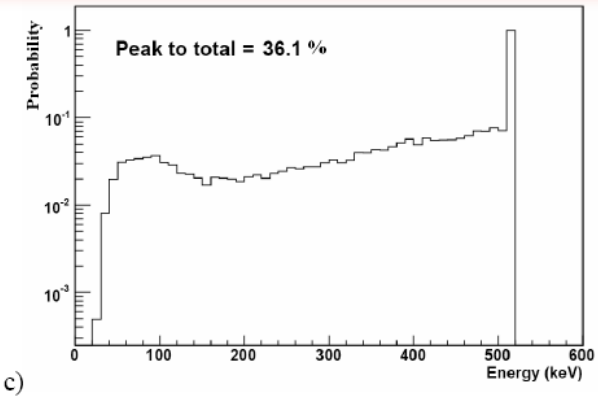

Fig.14. GEANT4 simulation: a 511 keV gamma source was simulated inside a water cylinder (20 cm radius, 180 cm height); a) energy response function of a MRPC with 400 µm thickness electrodes; b) normalised gamma energy spectrum obtained outside the cylinder. The peak to total ratio is only 12.6% due to the photon scattering into the water; c) energy spectrum of the interacting gammas that would generate detectable electrons into a MRPC array. The thickness of the MRPC electrodes cuts part of the low energy tail increasing the peak to total ratio up to about 36%.

Backscattering is important

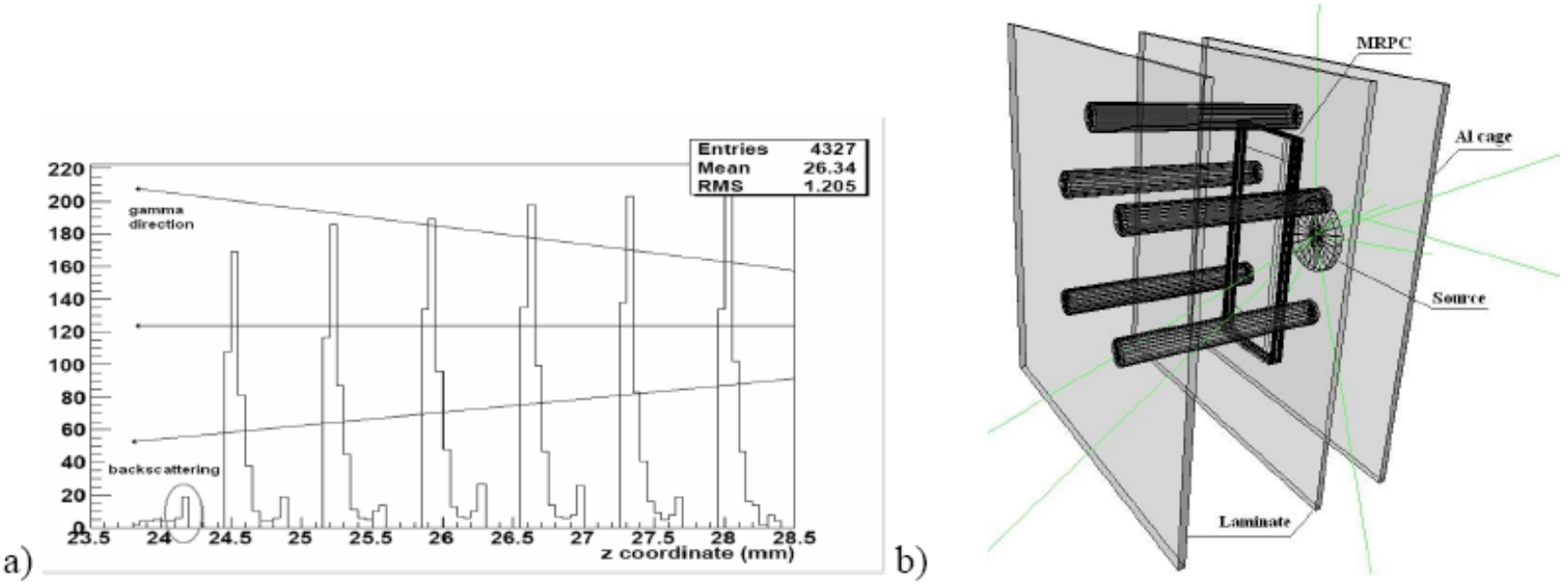

Fig.4 Results from a GEANT4 simulation of a 6 gaps glass MRPC: a) the depth of the photo produced and detected electrons is plotted. The 511 keV gammas come from the right and the peaks represent the last layers of the electrodes (that are 400 μm thick) in which the gammas are converted with following detection of electrons. The empty valleys represent the gas gaps (300 μm wide). Small peaks represent the initial layers of the following electrodes from which backscattered electrons are detected; b) GEANT4 geometry of the MRPC. Source, polycarbonate columns, laminate plates, the bottom aluminum cage are evidenced. Some gamma rays are also plotted.

[Vit06]

Sensitivity vs. FOV

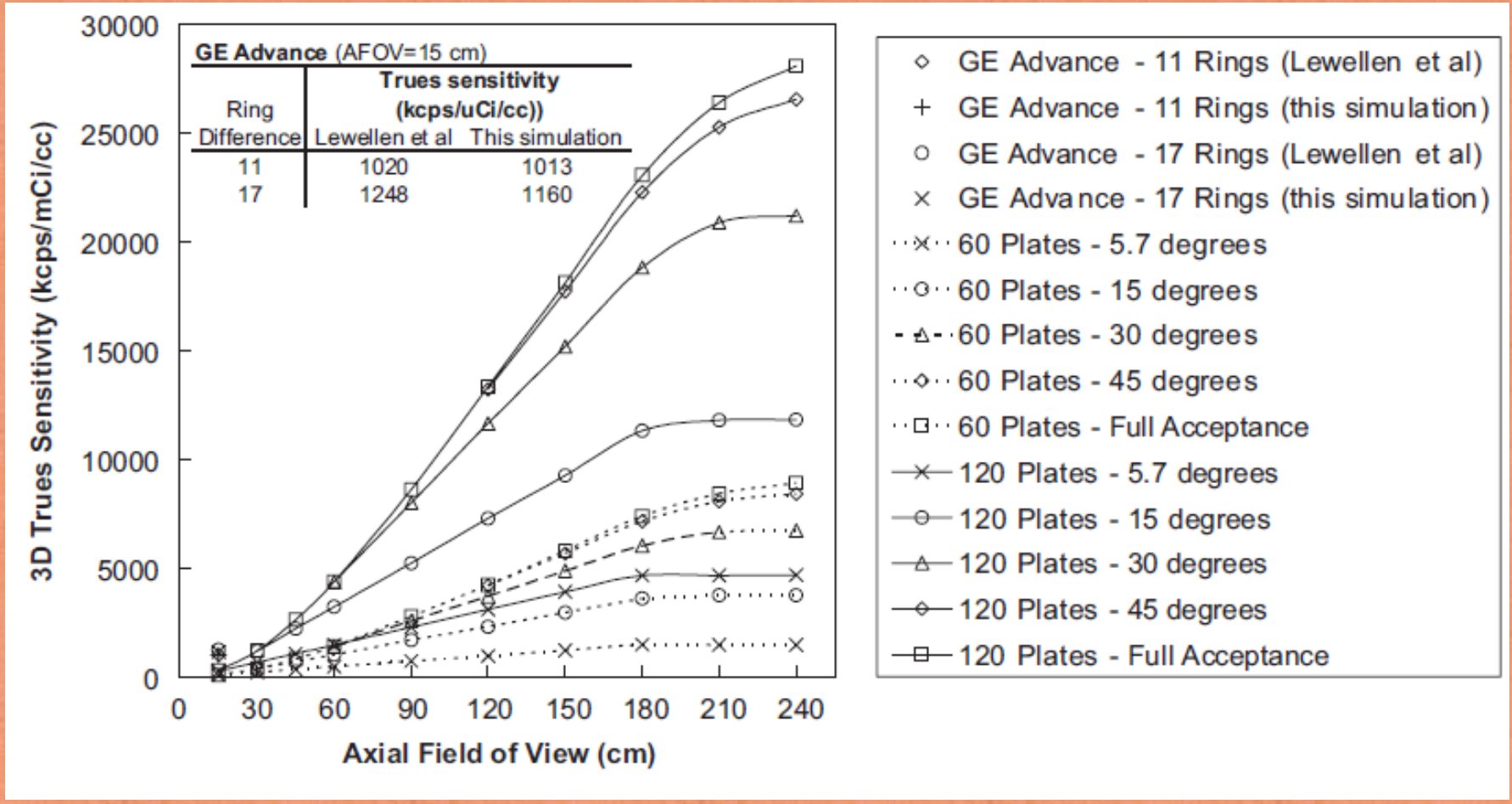

Simulated dependence of sensitivity from the FOV for different MRPC configurations compared to the GE Advance tomograph [Cou07][GEA].

Detectors performances for TOF-PET

Required	Crystals	MRPC
Time resolution (< 3 ns)	maybe	yes
Space resolution (< 1 mm)	yes	yes
Gamma detection efficiency	> 90 %	very low
Energy resolution	2-20 %	no
Price	BGO 50 €/cm^2	0.5 €/cm^2
Robustness and reliability	yes	yes
Easy of operation	yes	maybe

First application of PET – RPC (2004) (based on small animal PET requirement)

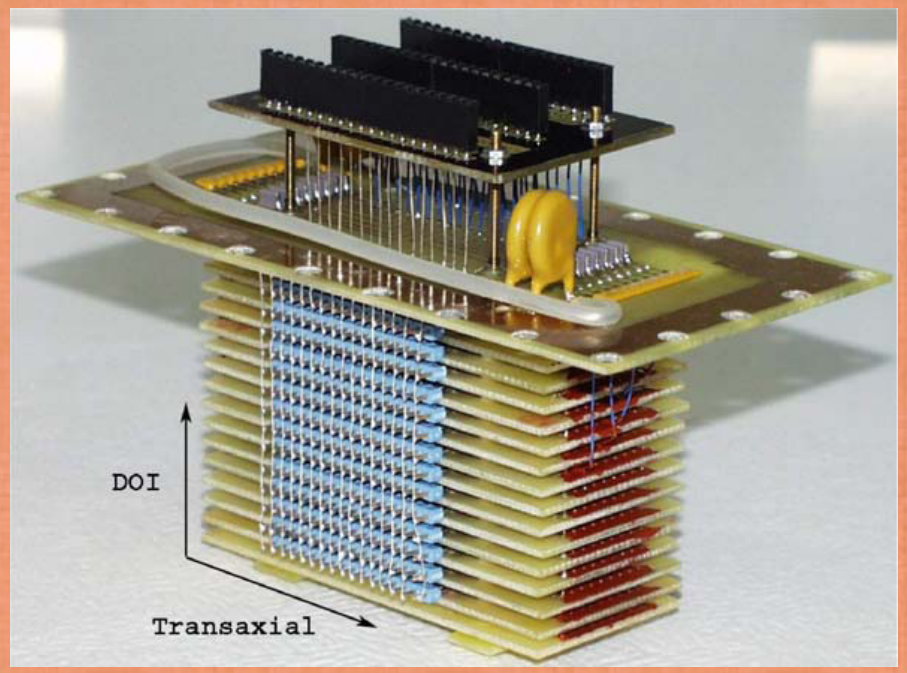

[Bla04]

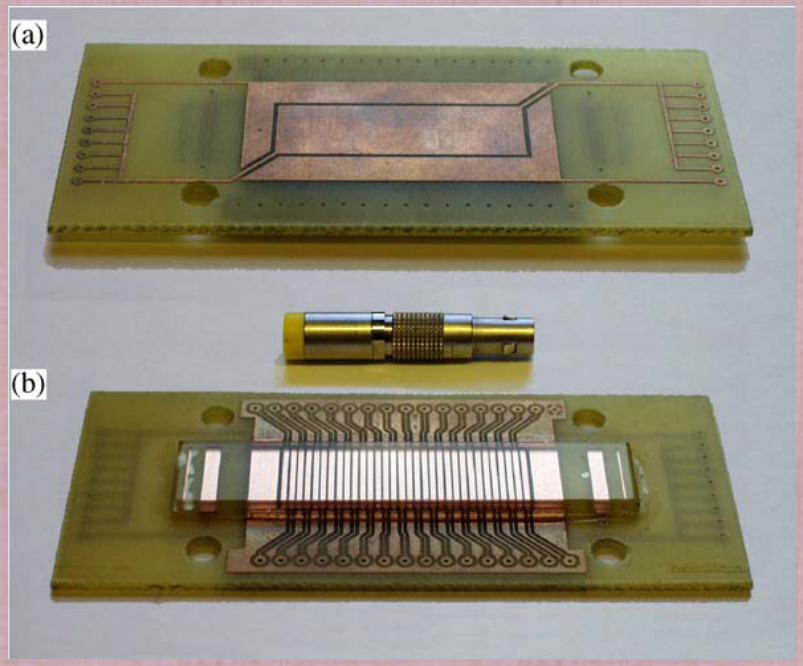

Made from PCB and accommodate in one side (a) the metallic cathode of an RPC(PC B copper), and on the opposite side (b) the 2mm thick glass anode of the next RPCand the 32 signal pickup strips, 1mm wide, which sense the transaxial dimension.

Results

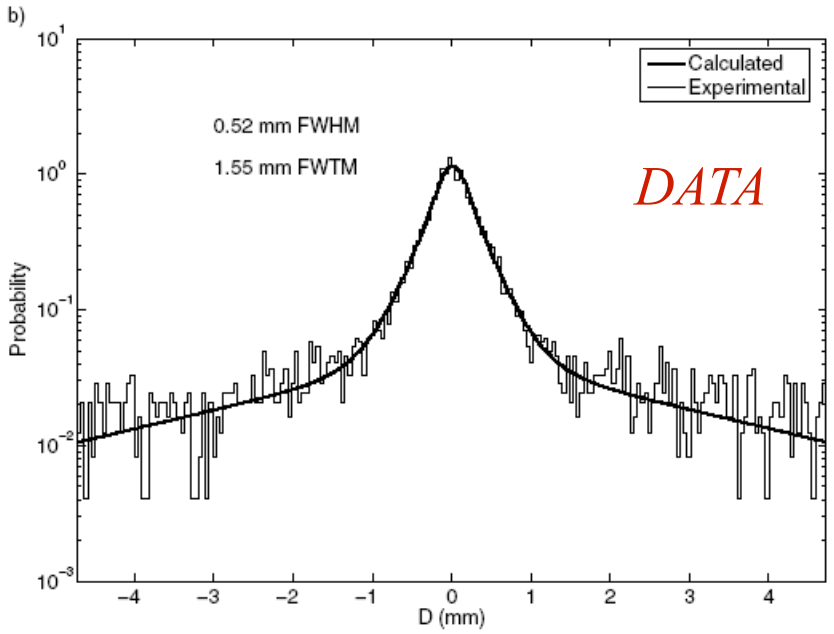

Fig.3. b) Experimental and calculated count distribution, showing a width of 0.52 mm FHHM and 1.5 mm FWTM.

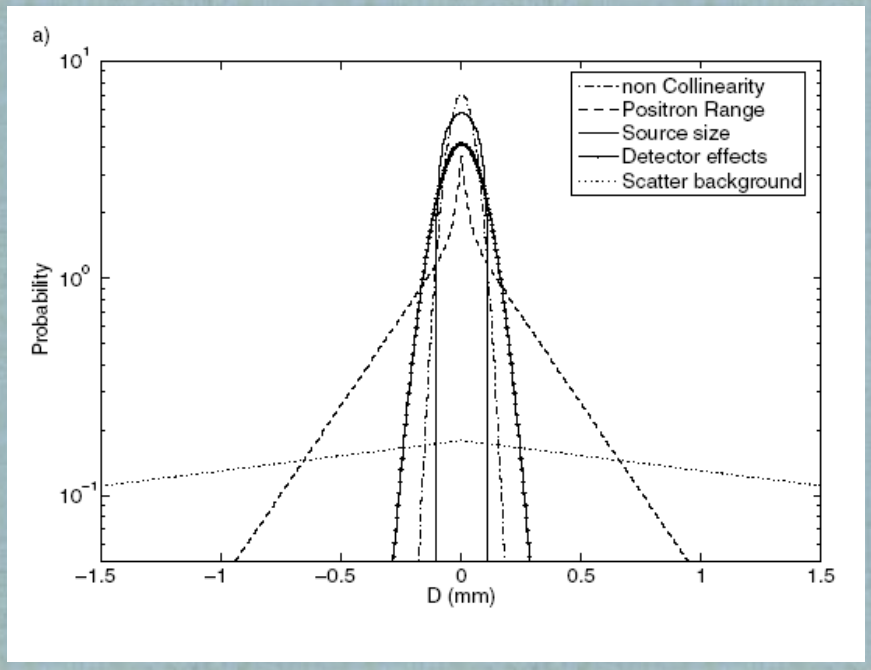

[Bla04]

•Annihilation photon non-collinearity: Gaussian distribution , *$N(x) = \exp(-x^2/2\sigma^2)$, $FWHM = 2.35\sigma = 0.0022ds$ (in mm), being ds the system* diameter (mm).

- Positron range: sum of two exponentials, *$P(x) = C_1 \exp(-k_1 x) + (1-C_1) \exp(-k_2 x)$ $x \geq 0$, k_2 free parameter*
- Detector effects: Modeled as a Gaussian distribution: *$D(x) = \exp(-x^2/2\sigma det^2)$, where σdet is a free parameter.*
- Source size: Modeled as a circle projection: *$S(x) = sqrt(size^2 - x^2)$; where size is the source radius (mm).*
- Scatter background: Modeled as exponential *$SC(x) = C_2 \exp(-k_3 x)$, $x \geq 0$, where C_2 and k_3 are free parameters.*

Results

Duoble peak resolution

[Bla04]

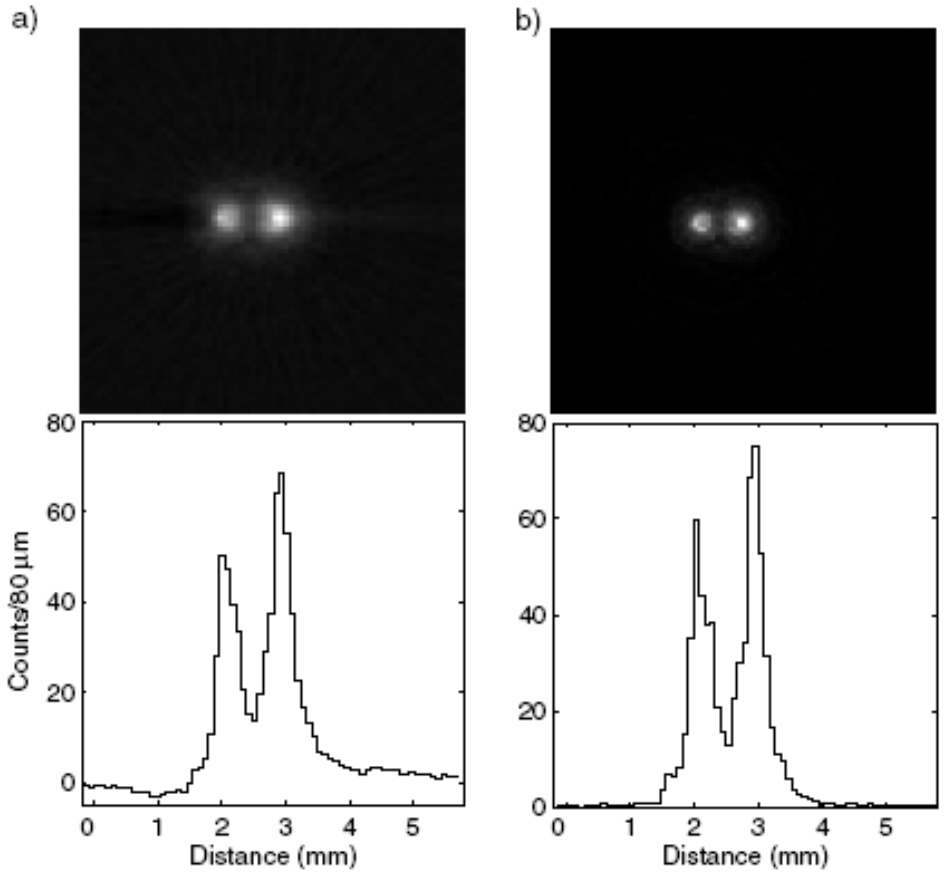

Fig.4. Image reconstruction, using two different algorithms a) The standard algorithm of filtered back projection (FBP) and b) maximum likelihood–expectation maximization (ML-EM) type algorithm. Both algorithms show the two central sources clearly resolved, in good agreement with the reconstructed spatial resolution, determined from the individual sources, of 0.5 mm FWHM and 0.4 mm FWHM for the FBP and ML-EM respectively

Our Prototype layout

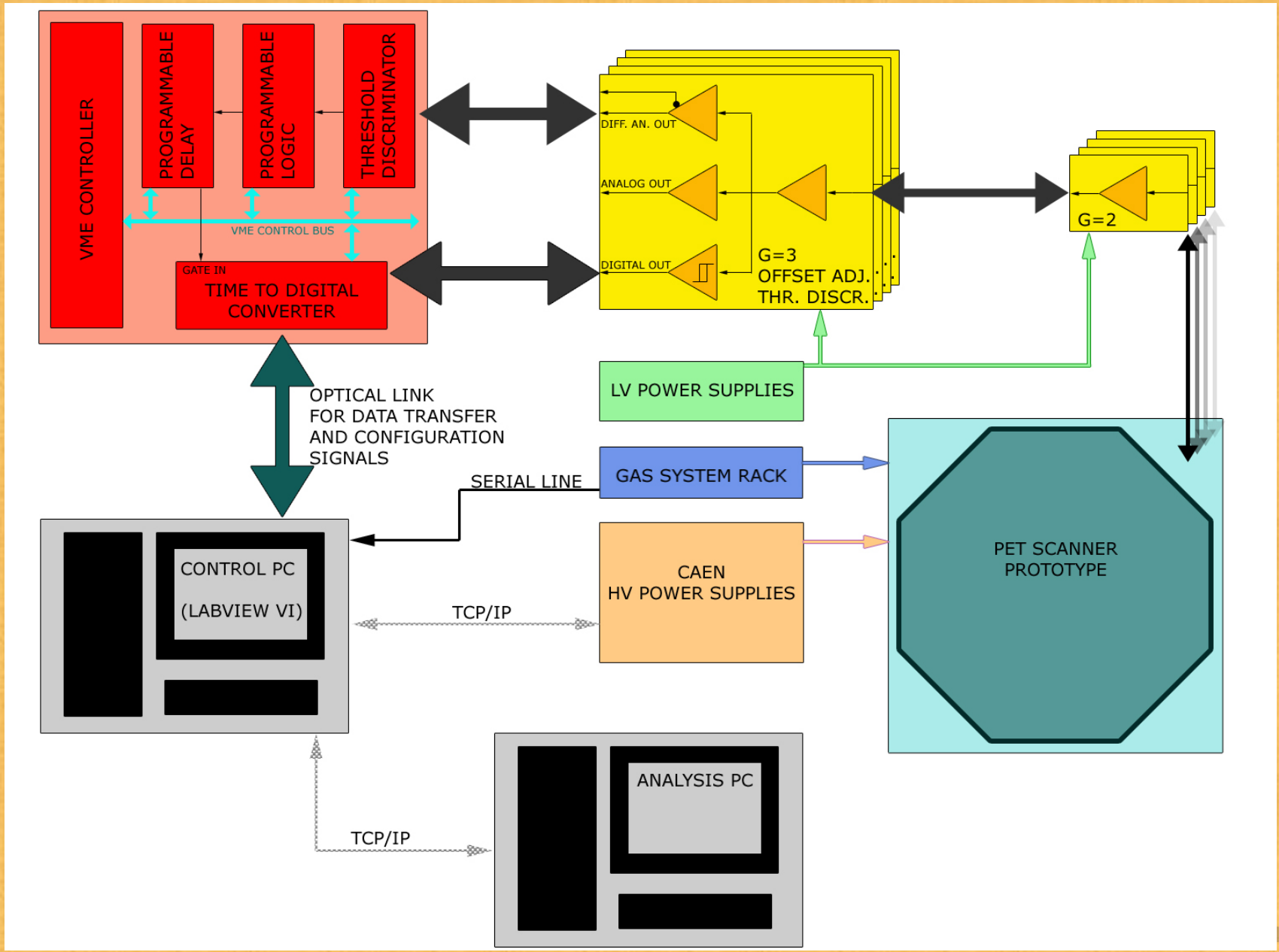

Prototype description – detector

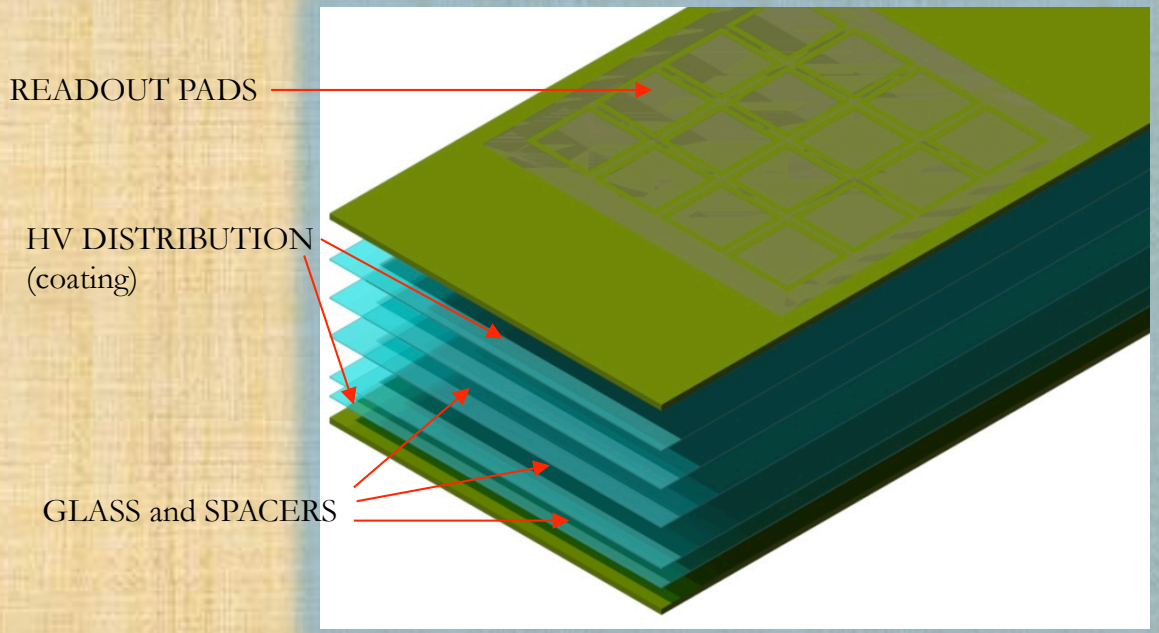

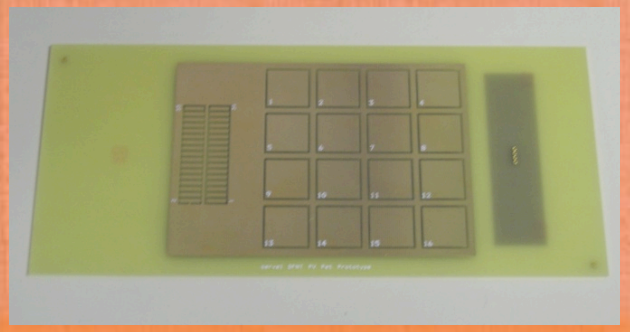

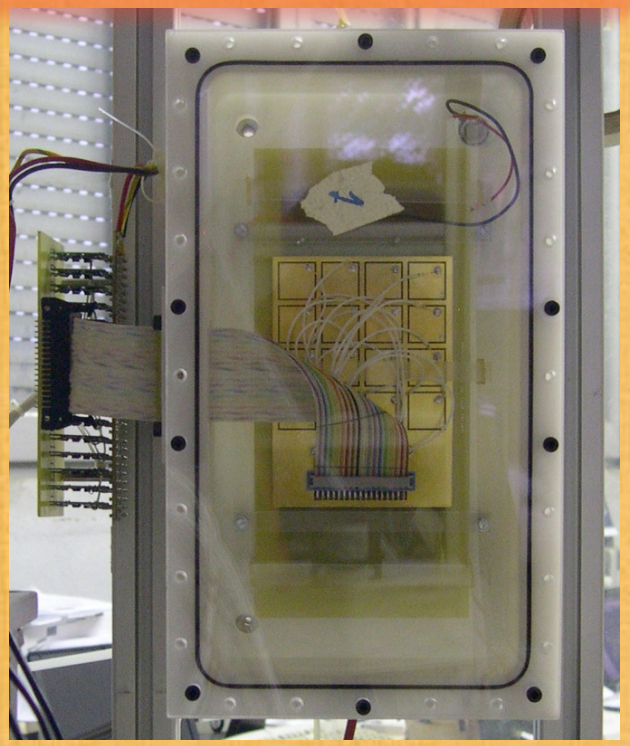

- 16 pads (1.6 x 1.6 cm^2)
- 4 gas gaps 250 µm
- 400 µm glass
- 5-25 MΩ resistive coating
- iC_4H_{10}, SF_6, $C_2H_2F_4$ (5 %, 10 %, 85 %)

Coating: why it is important.

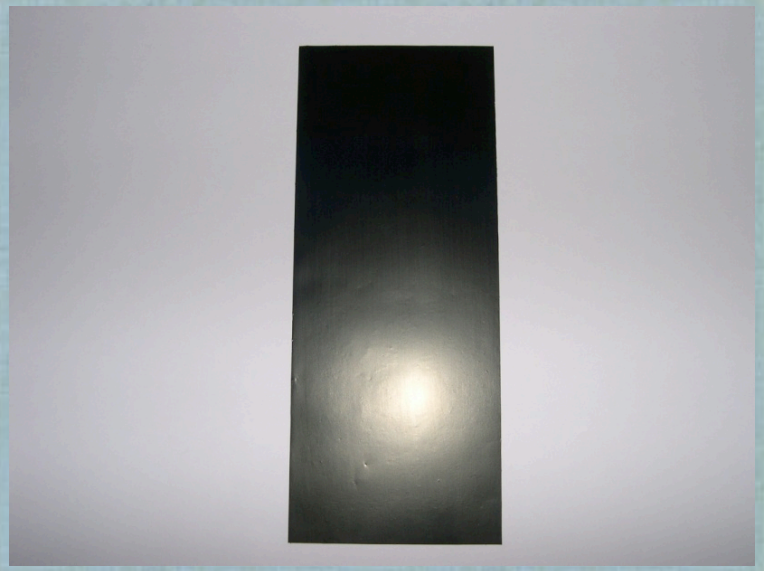

1) *The coating must distribute the HV*
2) *The coating has to be transparent to the signal*

3) *We use a carbon-black based paint*

Prototype description – geometry

Prototype stage 1: mechanical frame. 2 MRPC (ToF capabilities demonstration)

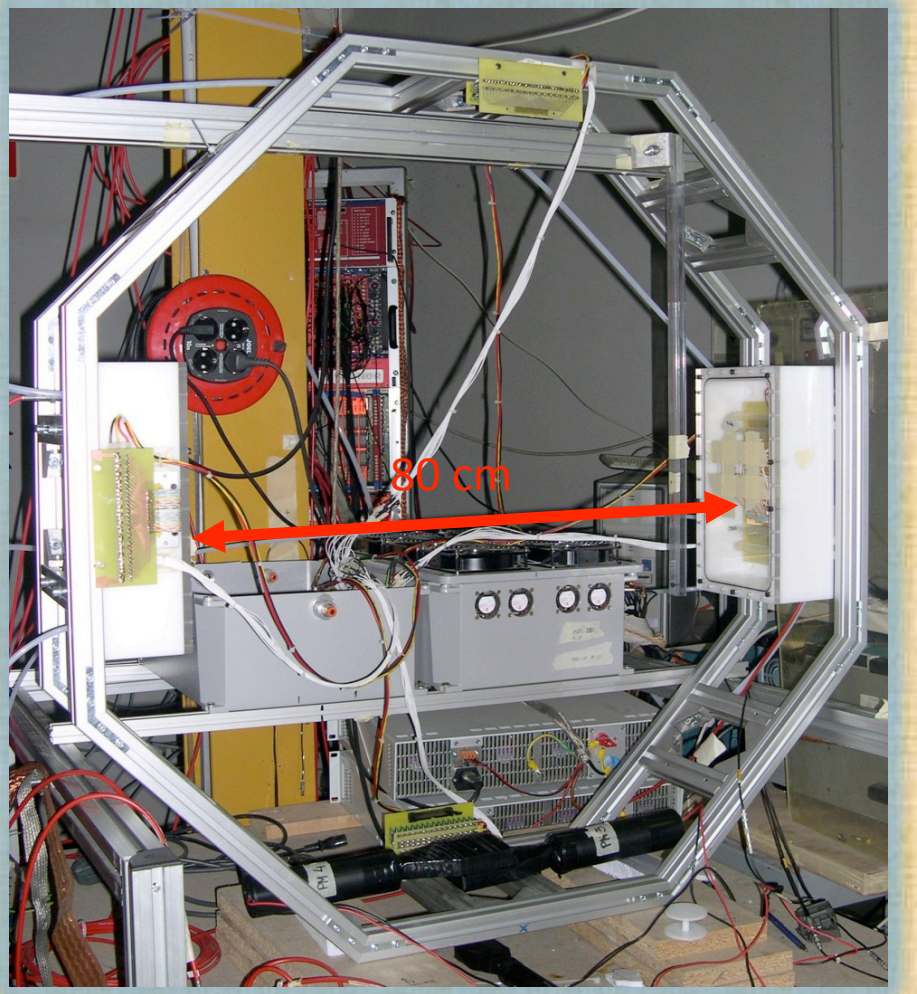

Prototype stage 2: 4 MRPC – Imaging capability WORK IN PROGRESS

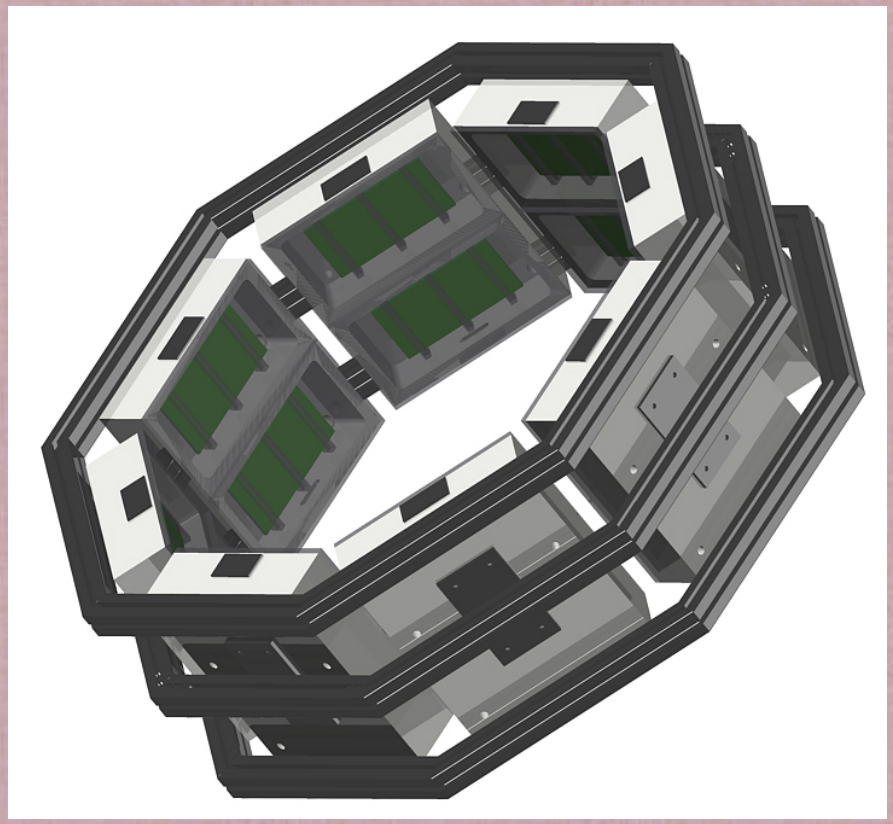

Prototype stage 3: Fully popolated ring

Prototype description – electronics

- Front-end:
  - Signal amplification
  - Noise rejection
  - Offset correction
  - Differential conversion
  - Digital conversion
- DAQ is performed using commercial CAEN modules
- Currently each readout channel is read by its own front-end.
- Not suitable for a full scale tomograph (≈5 m^2→ over 10^4 readout channels: price and complexity reasons).
- Possible solution: multiplexing
- Several readout chips developed for HEP feature multiple readout, shapers and discriminators.

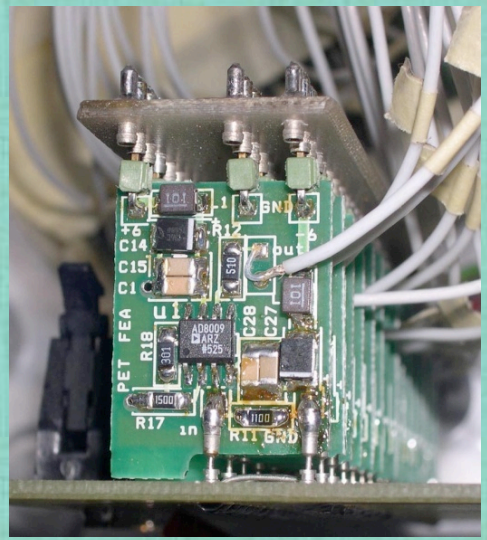

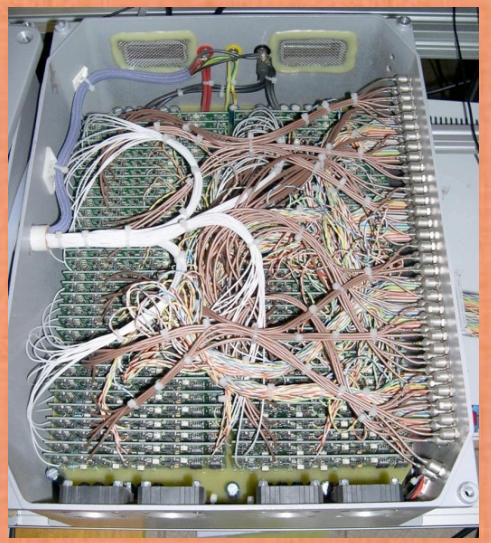

Prototype description – software

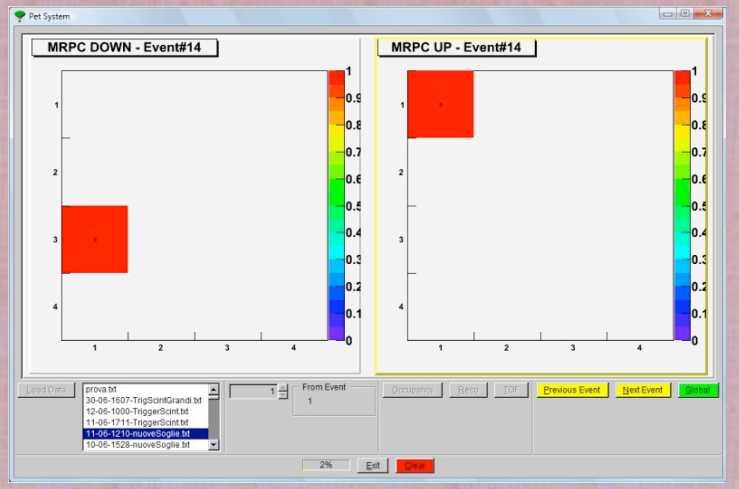

LOR definition

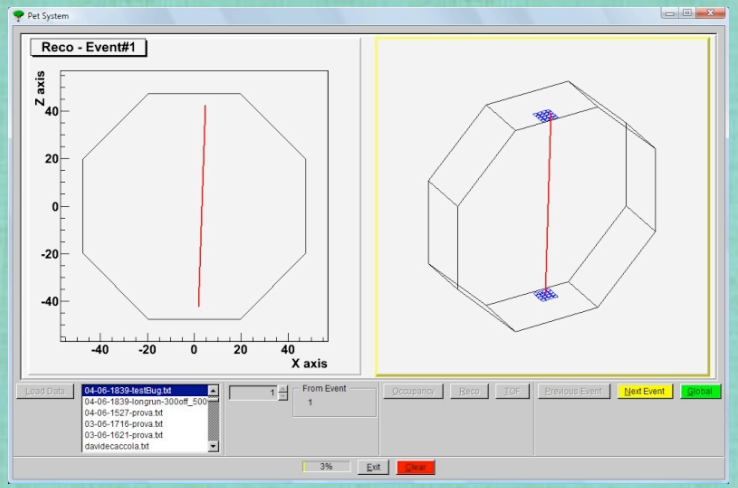

Data acquisition and detector control

A LabVIEW state machine controls the state of HV, the configuration of the DAQ system and saves the data to disk.

Further tasks (efficiency measurements, waveform storage, online data analysis) available.

Efficiency test with cosmic rays

Why?

- *Test MRPC geometry and construction*
- *Determine working point*
- *Gas mixture studies*
- *Test of resistive coating*
- *Threshold measurements*

1 gap Efficiency

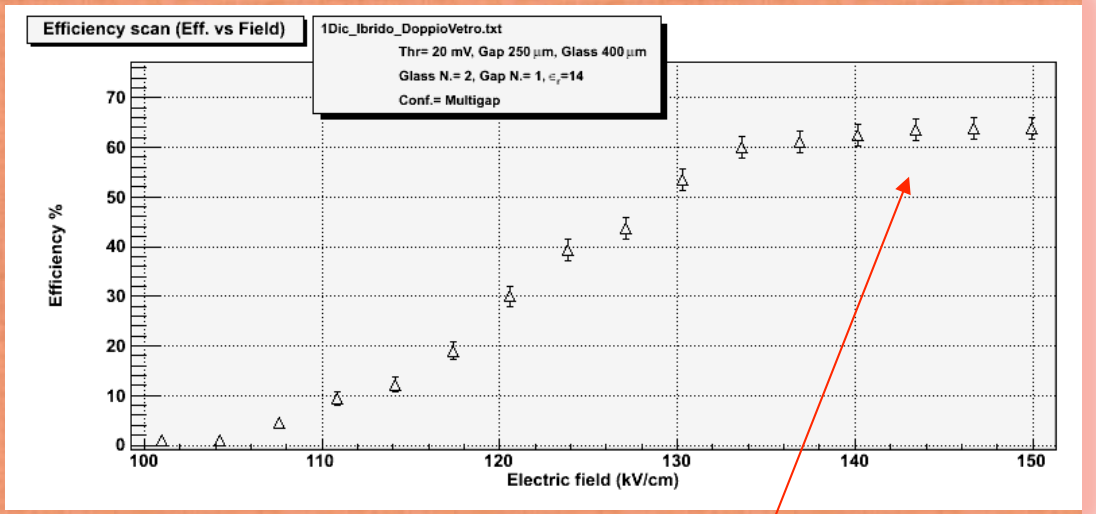

$$\varepsilon = 1 - e^{-\lambda d\left(1-\frac{\eta}{\alpha}\right)}\left[1+\frac{\alpha-\eta}{qE_w}Q_t\right]^{\frac{\lambda}{\alpha}}$$

[Abb]

$\varepsilon_{theor} = 64\ \%$

$\varepsilon_{meas} = 63.2 \pm 0.7\ \%$

Efficiency tests with gammas

- To obtain a reliable trigger a ^{22}Na source is used in conjunction with NaI(Tl) crystals.
- Trigger is valid when both a 511 keV and 1274 keV photons are detected.

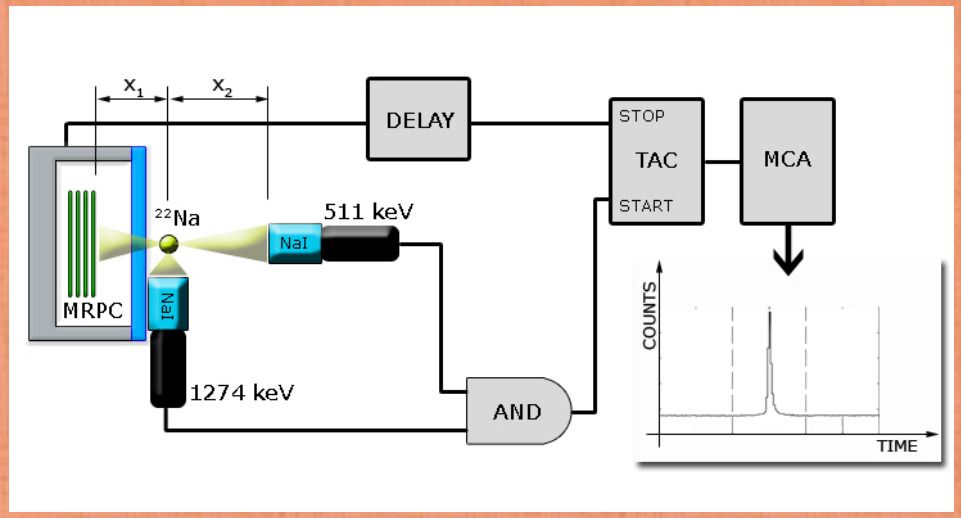

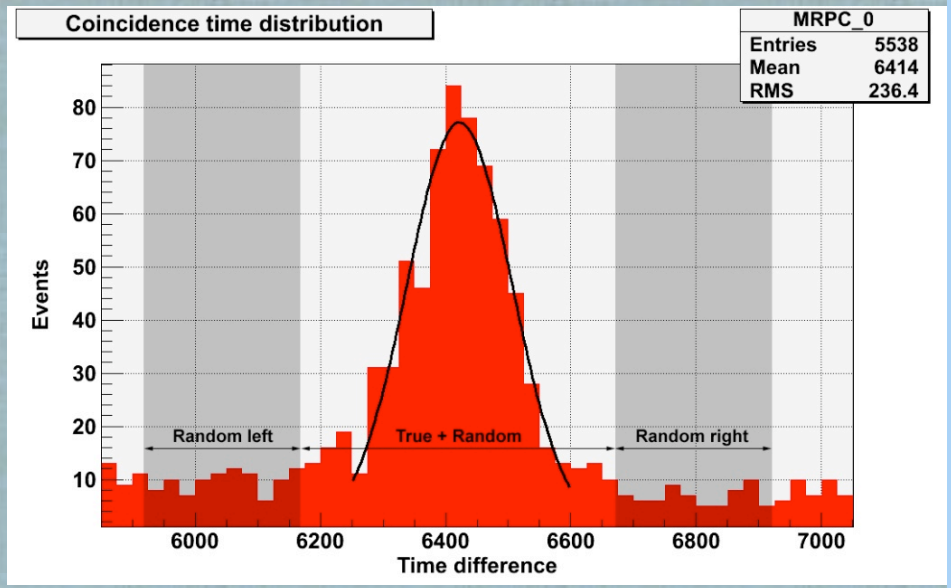

$$\varepsilon = \frac{N_{True+Random} - N_{Random\_left} - N_{Random\_right}}{N_{trigger}}$$

Time resolution to (511 keV) gammas

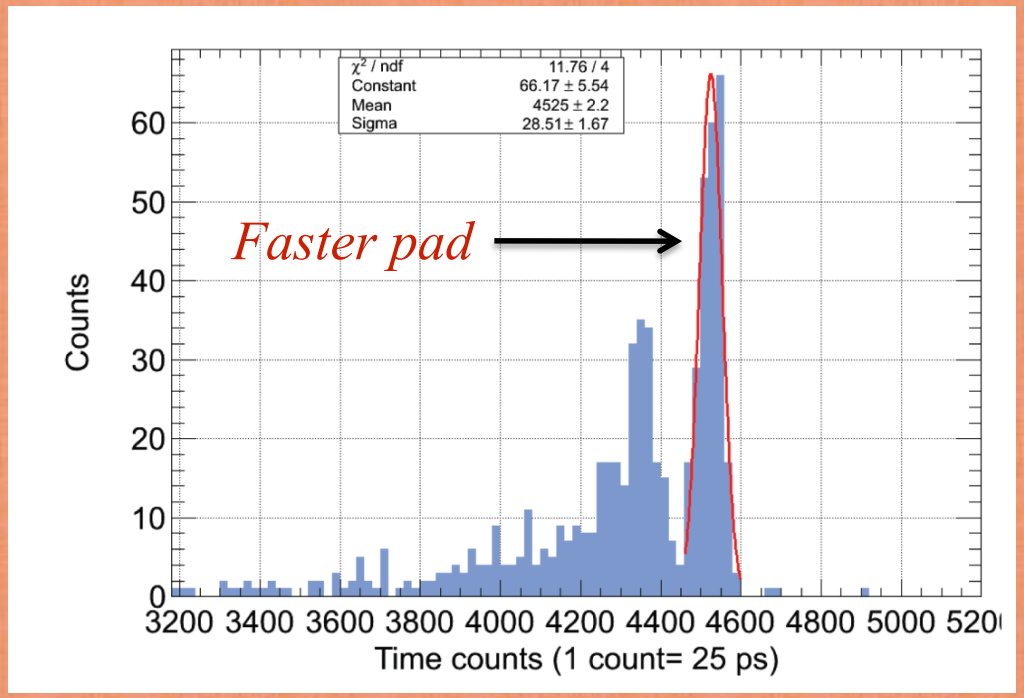

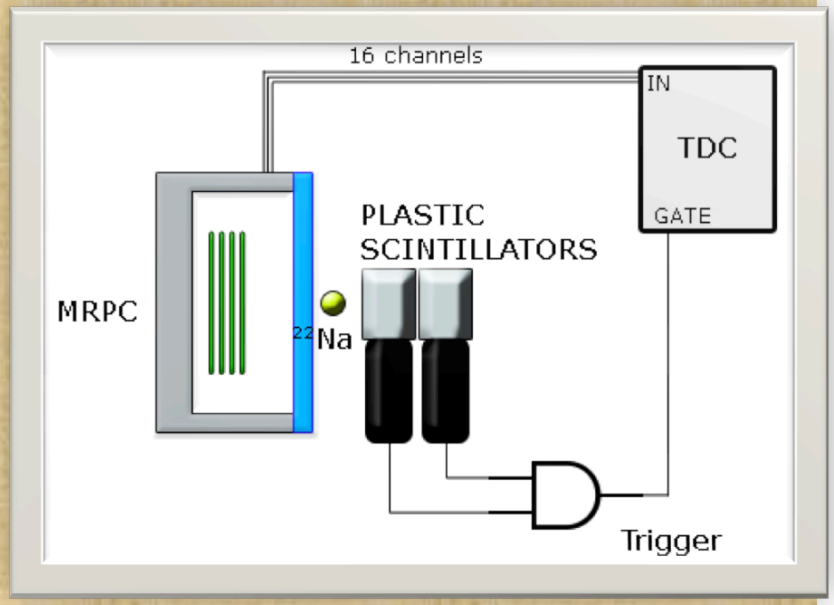

Averaging on all the pads we obtain

σ_t= 450 ± 40 ps (@ 11 mV eq thr)

(not amplitude corrected)

[Vit09]

Meanwhile we are testing a NEW Electronics Test (x 10 amplification) Typical signals

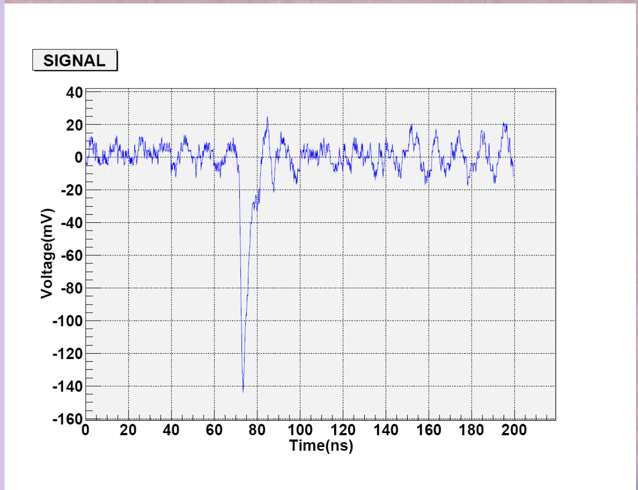

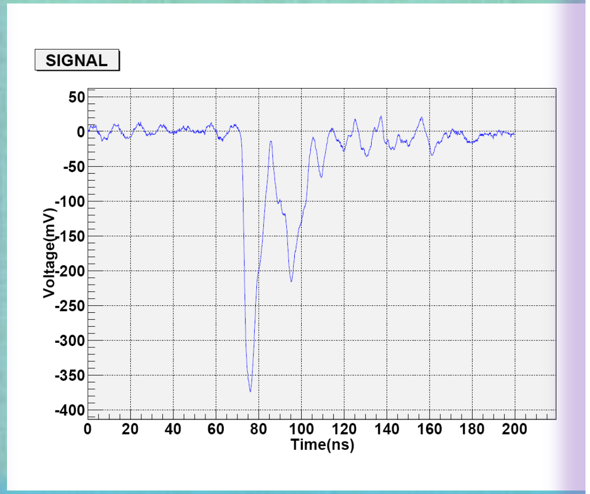

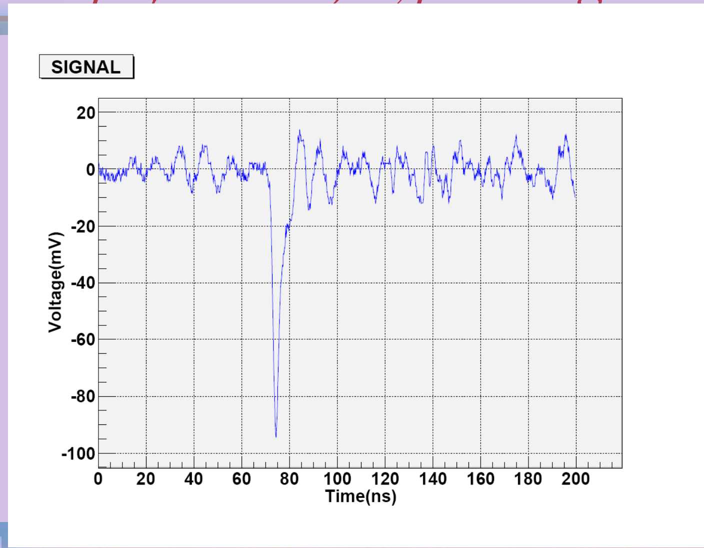

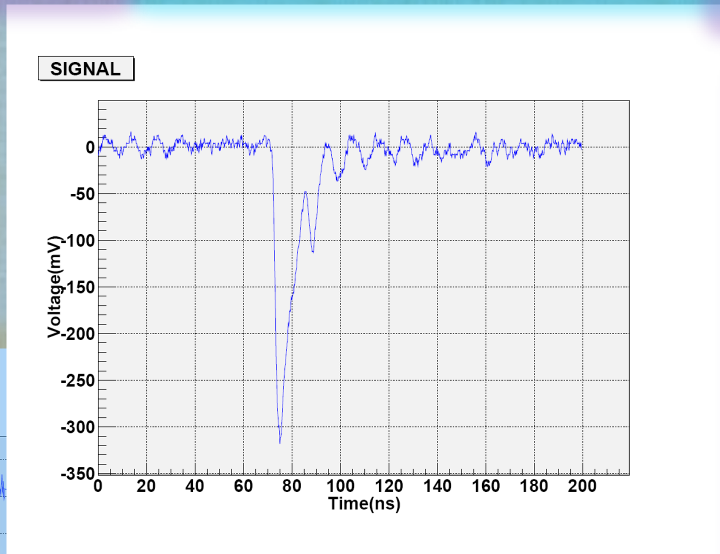

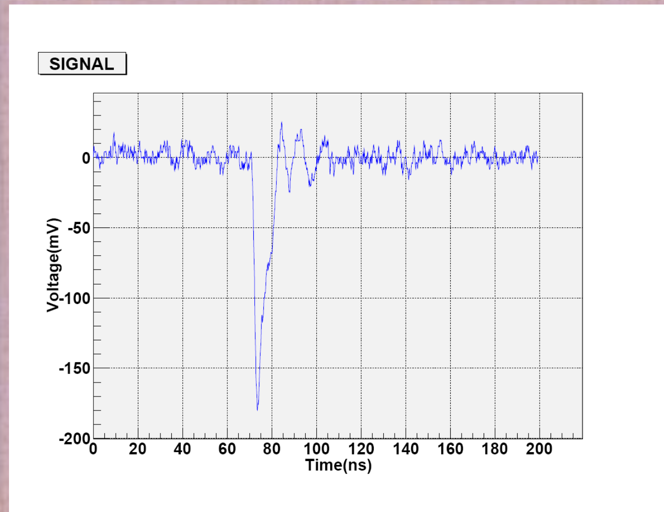

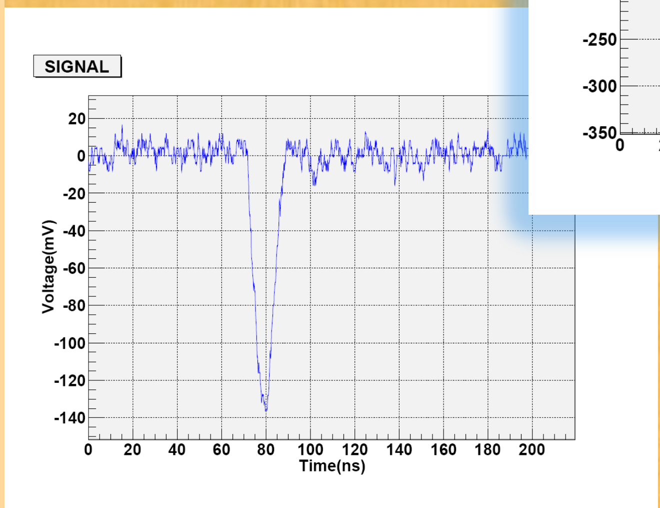

Environmental background (we have chambers with plastics case)

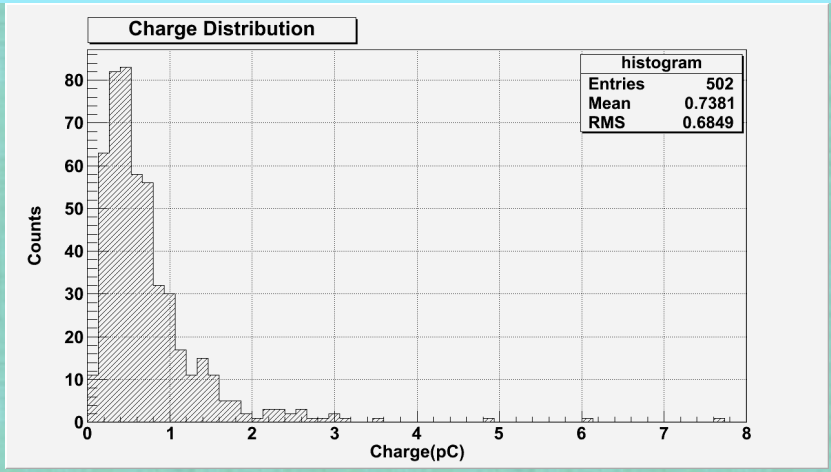

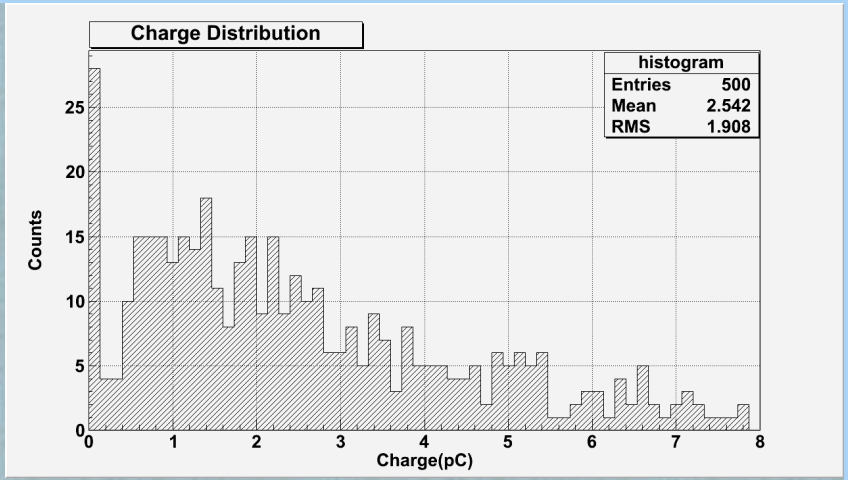

Efficiency and charge distribution of 4 (250 um) gaps MRPC

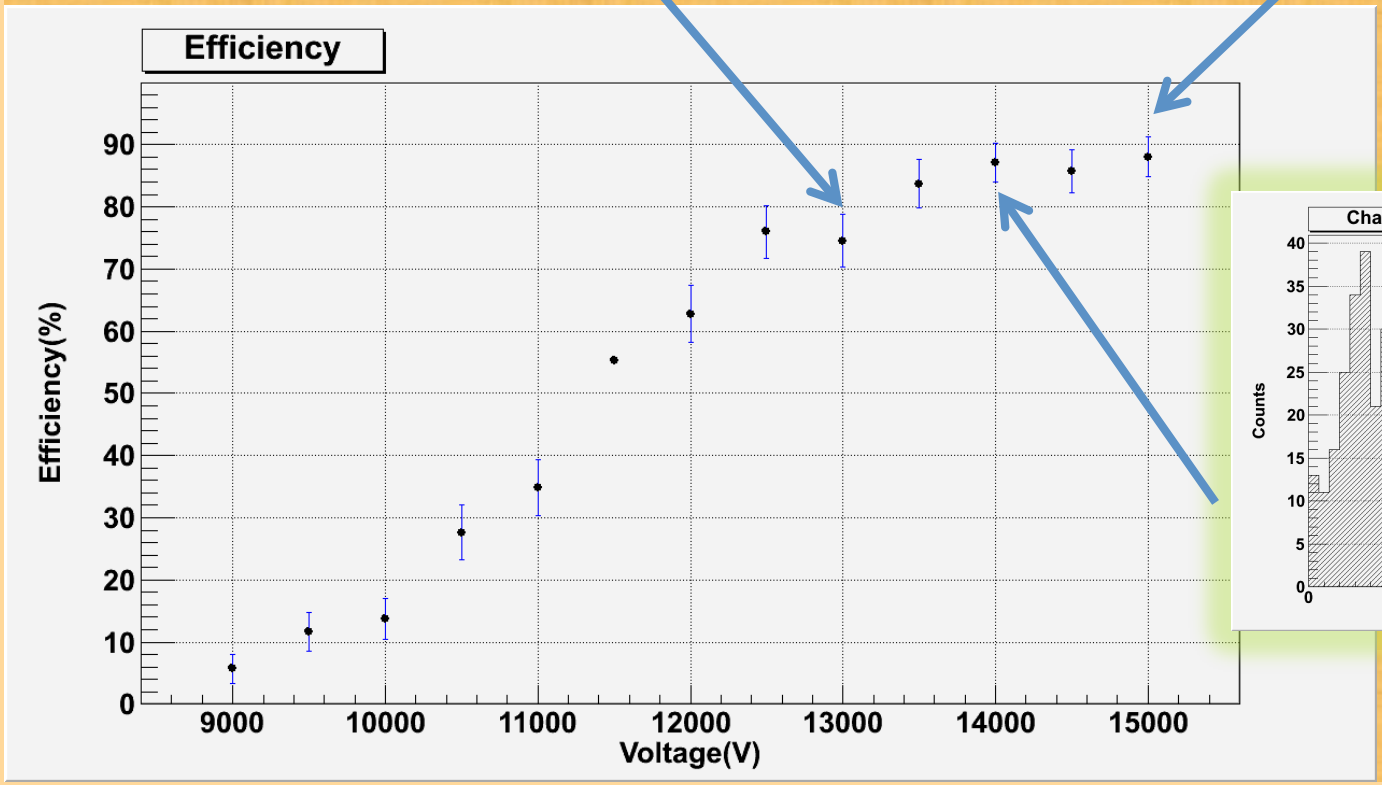

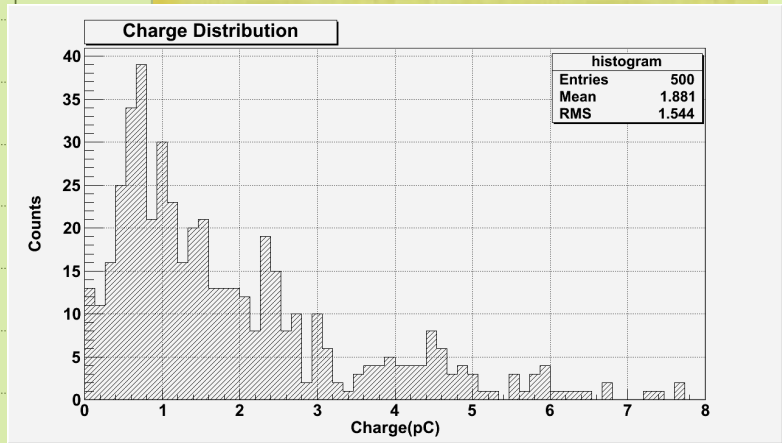

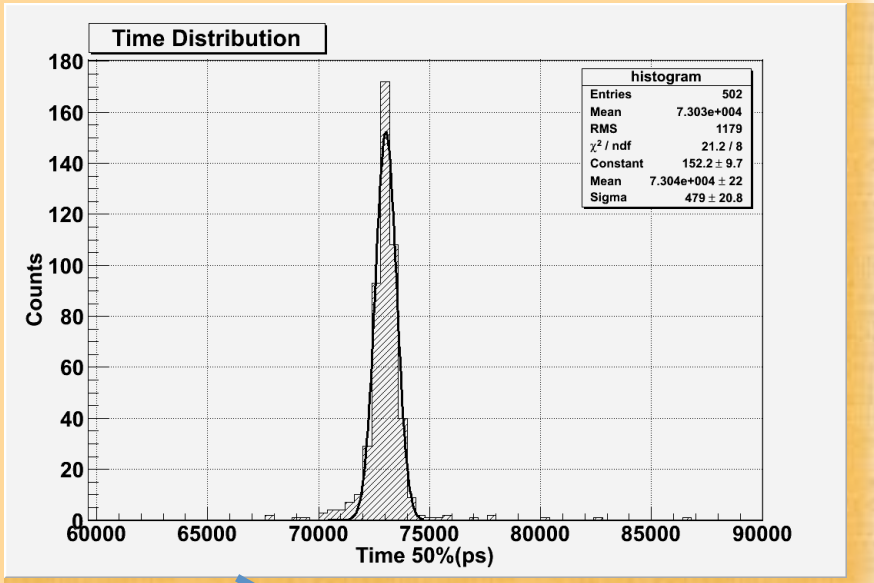

Cosmics

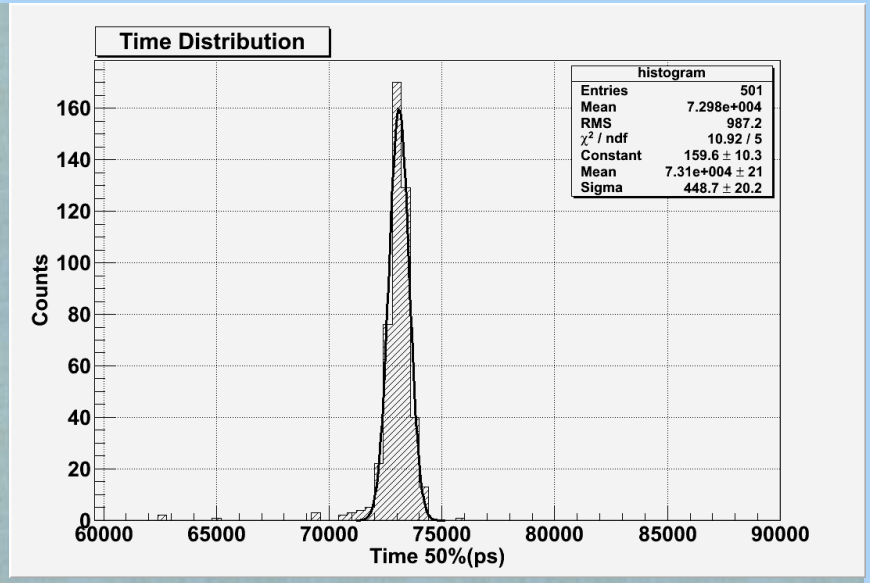

Efficiency and time distribution of 4 gaps (250 um) MRPC

$$\sigma_{obs} = \sqrt{\sigma_{MRPC}^2 + \sigma_{Trig}^2} = 400\,ps$$

$$\sigma_{Trig}^2 = \sigma_{MRPC}^2 \Rightarrow \sigma_{MRPC} = \frac{400}{\sqrt{2}} \approx 284\,ps$$

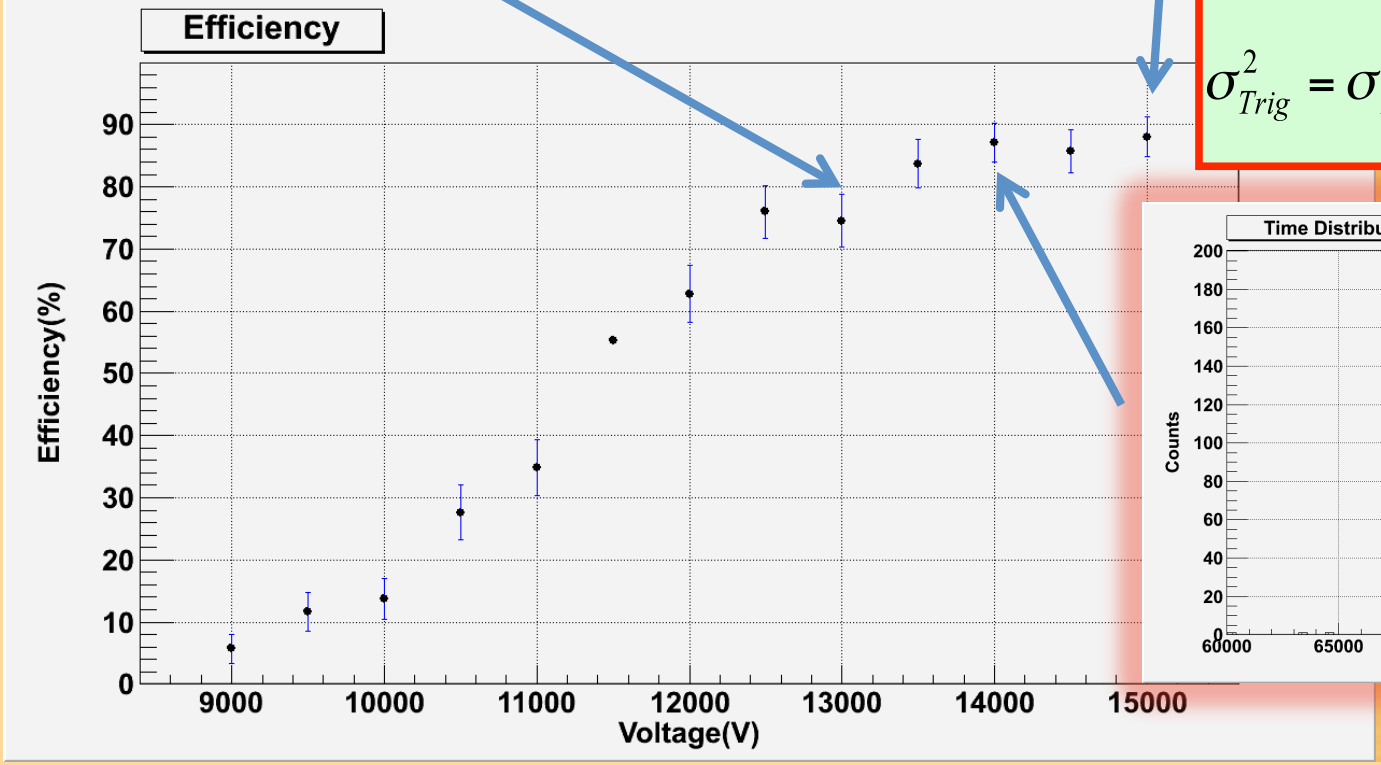

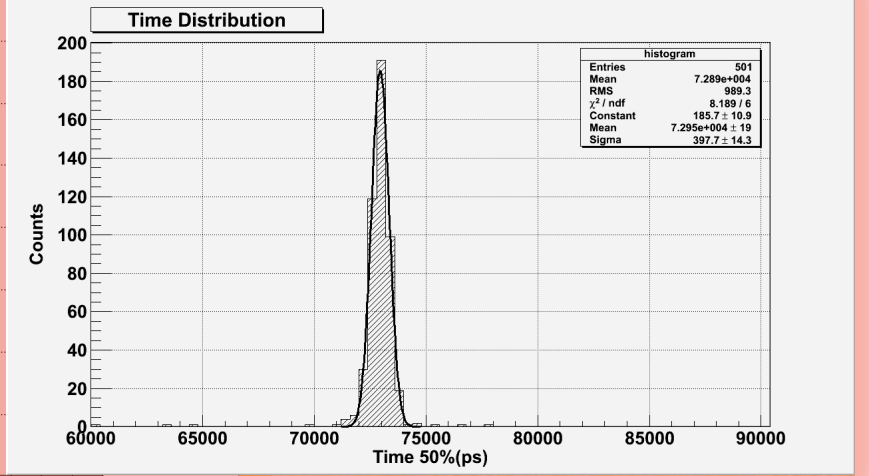

Conclusions and developments

- σ_t= 450 ps leads to a sensitivity gain G_χ
  - $G_\chi \approx 3$ for head (d= 20 cm)
  - $G_\chi \approx 7$ for torso (d= 50 cm)
- Increase FOV to 200 cm leads to $G_\chi = 10 \div 20$
- A (conservative) average gain of $G_\chi = 25$ is well within the possibilities of full-body RPC TOF-PET
- A single detector efficiency $\varepsilon \approx 20$ % is reasonable to obtain a scanner with performance comparable to crystal-based scanners

Conclusions and developments

- A multi-stack MRPC seems a convenient way to obtain the required efficiency. N≈ 200 gaps (about 25 cm thick detectors)
- Depth Of Interaction information can be obtained
- A detailed analysis of efficiency vs. energy is required to determine the scattered coincidences contribution

References

[Bad] Badawi et al., IEEE transactions on nuclear science, Vol. 47, issue 3 (2000)

[Abb] Abbrescia et al., Nucl. Instr. And Meth., A431 (1999) 413-427

[Cou07] Couceiro et al., Nucl. Instr. And Meth., A580 (2007) 915–918

[Vit06] Vitulo et al, SIF2006 + Unpublished Data

[GEA] Lewellen et al., IEEE transactions on nuclear science, Vol. 43, issue 4 (1996)

[Ame] Ametamey et al., Journal of nuclear medicine, Vol. 48, issue 2 (2007)

[Rad] Radu et al., Nature medicine, Vol. 14, issue 7 (2008)

[Lip] Lippman et al., Nucl. Instr. And Meth., A602 (2009) 735–739

[Bla04] A. Blanco et. Al., Nucl. Instr. And Meth., A533 (2004) 139–143

[Knoll] F.G. Knoll, Radiation Detection and Measurement (John Wiley & Sons)

[Chid] K.Chidlow,T.Moller , Rapid Emission Tomography Reconstruction

[Muller] J.W. Muller, Generalized Dead time, Nucl. Instr. And Meth., A301 (1991) 543–551

[Bla09] A. Blanco et al., Nucl. Instr. And Meth., A602 (2009) 780–783

[Vit09] P. Baesso et al., IEEE09 , Orlando (FL)

[Tow04] D. Bailey, D. Townsend,P.E.Valk, M.N.Maisey Ed., PET, Springer 2004

Alice –TOF MRPC (10 gaps 250 um)

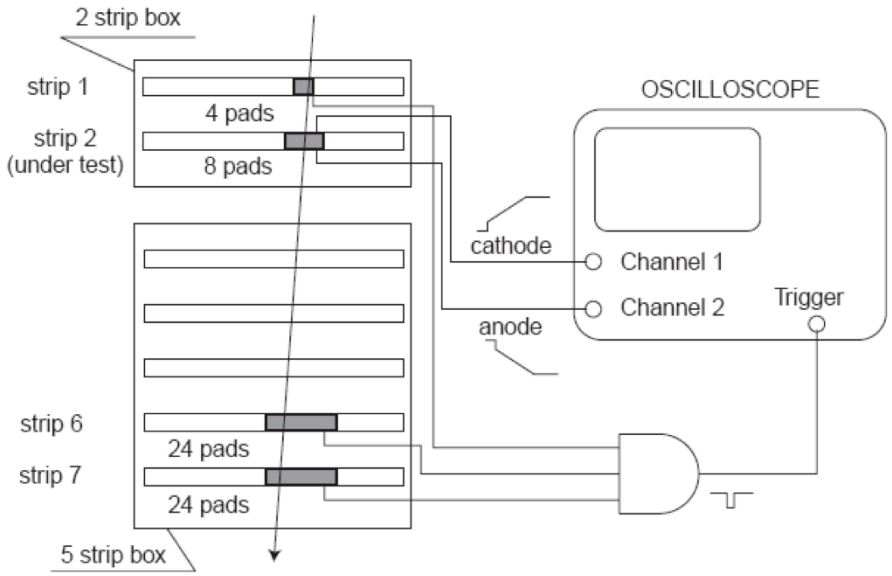

Fig. 2. Experimental setup used for the measurement of the MRPC charge with cos

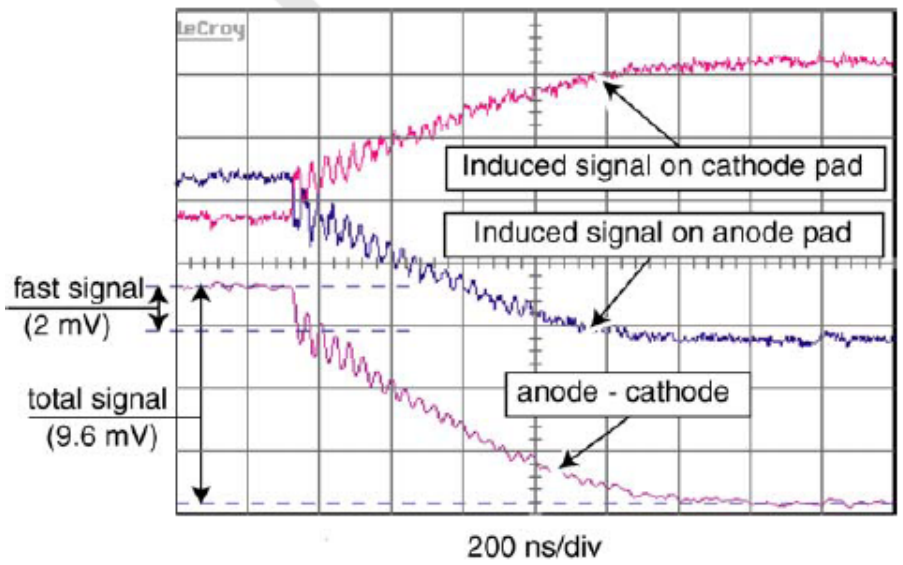

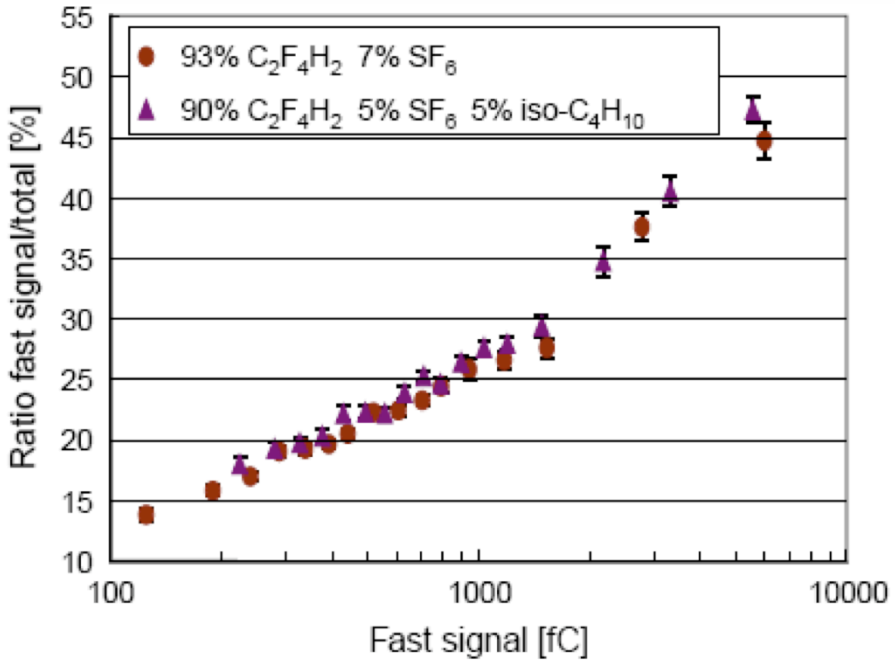

Fig. 5. Ratio of the fast charge to total charge as a function of fast charge.

Electric field inside the gap

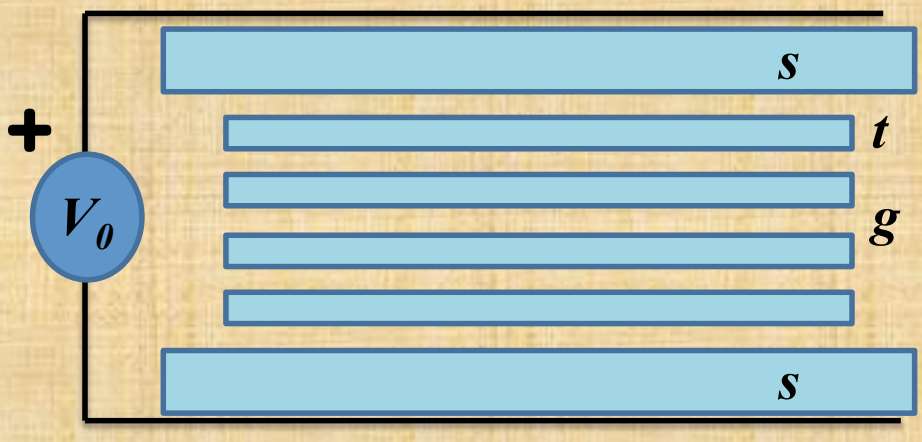

$$E_g = \frac{\varepsilon_r}{2s + (n_g - 1)t + n_g g \varepsilon_r} V_0$$

E_g	electric field inside the gap
V_0	external applied voltage
s	external electrodes thickness
t	floating electrodes thickness
g	gap width
n_g	number of gaps
ε_r	dielectric permettivity

CMS-RPC: E_g(s =t=g=2mm; n_g=1 ; V_0 = 9.4 kV ; e_r=5) → 35.6 kV/cm

Read-out geometry

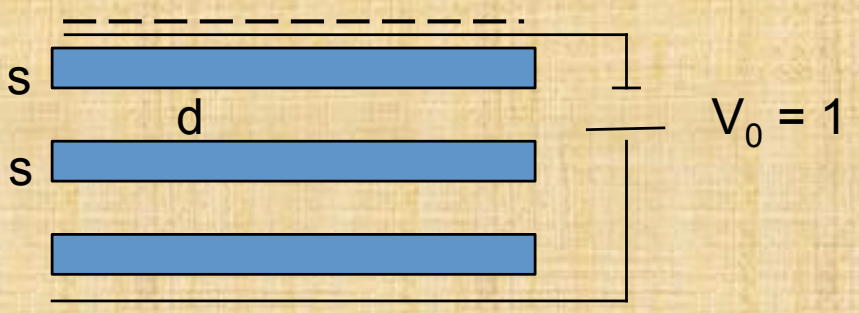

"Common Read-out"

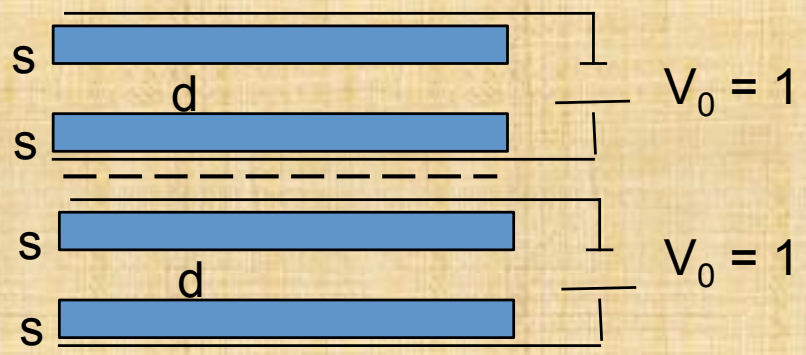

$$k = \frac{\varepsilon_r d / s}{2\varepsilon_r d / s + 3}$$

$$k = 2 \times \frac{\varepsilon_r d / s}{\varepsilon_r d / s + 2}$$

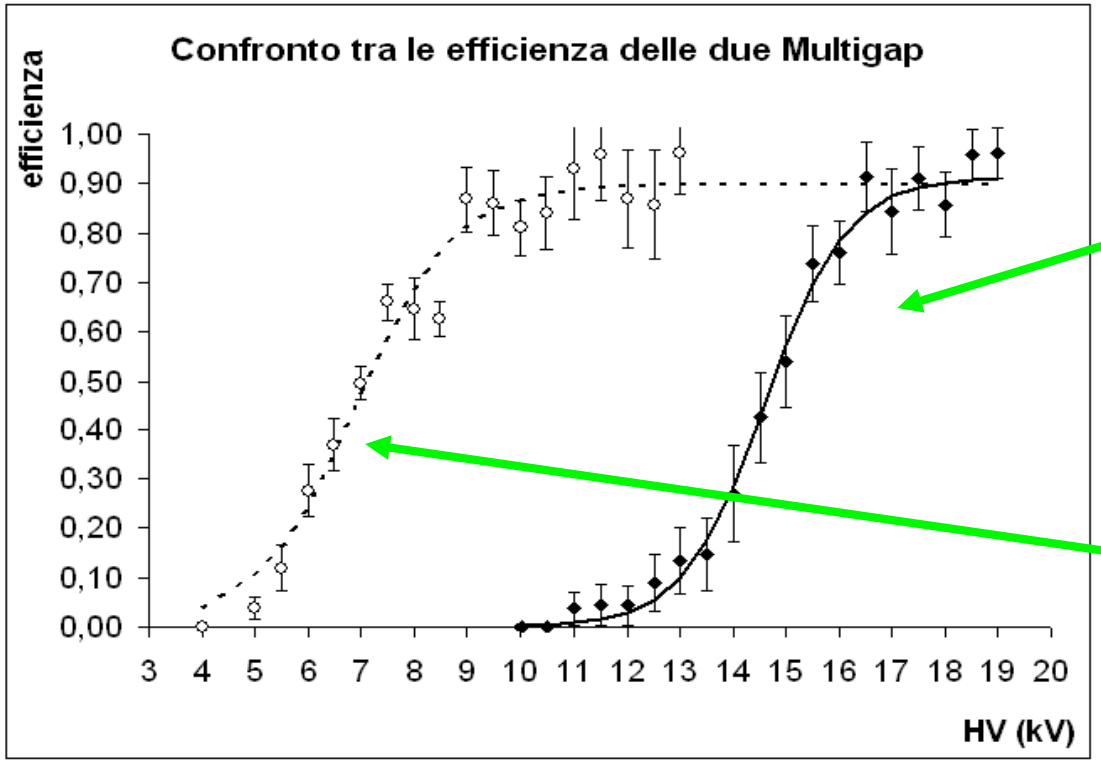

1mm External Electrodes

400 um External Electrodes

[Vit 06]

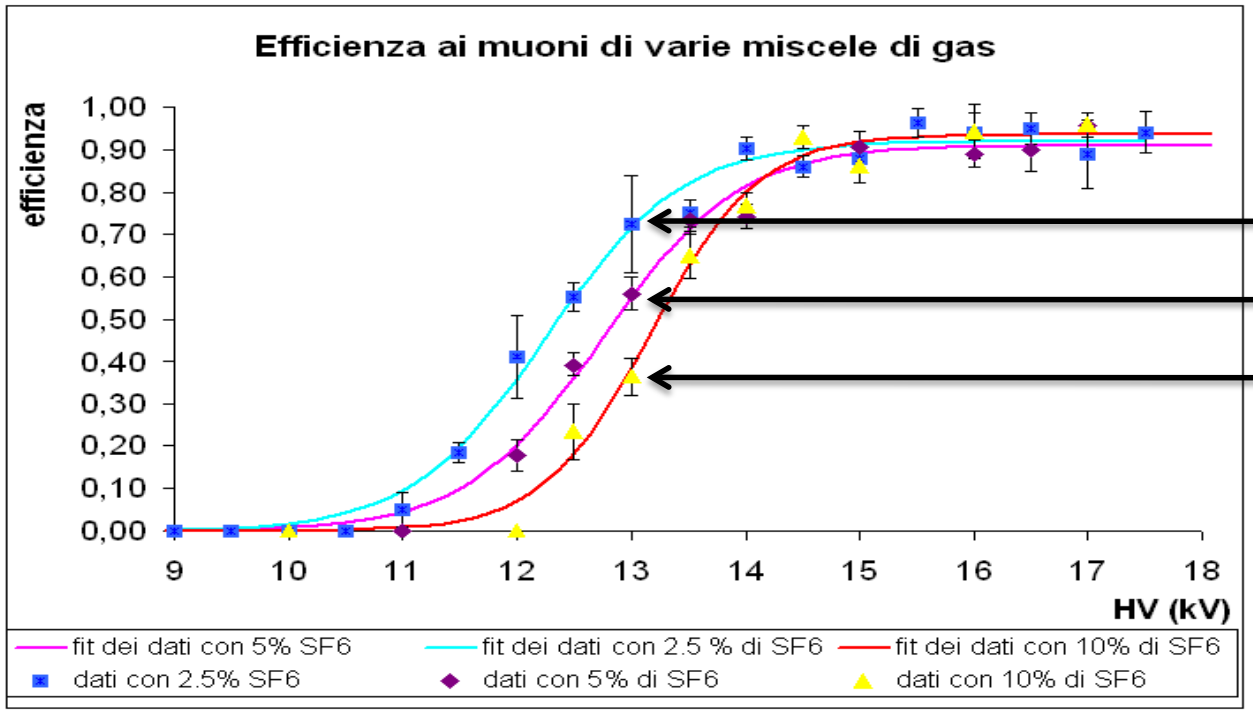

2.5 % SF6
5% SF6
10% SF6

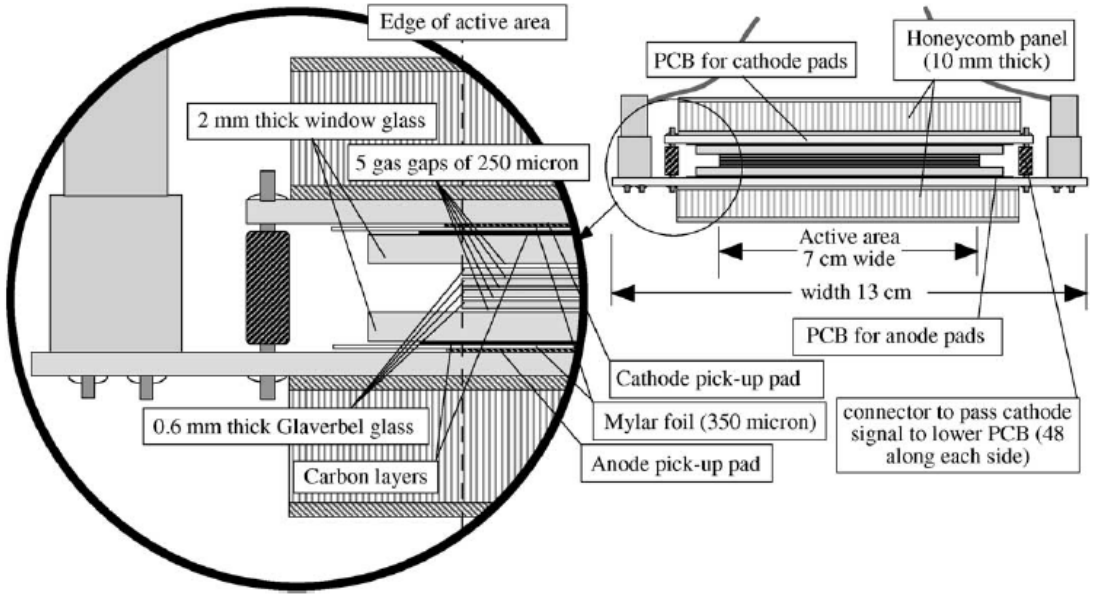

Fig. 2. Cross-section of MRPC strip with 96 pads for the readout.

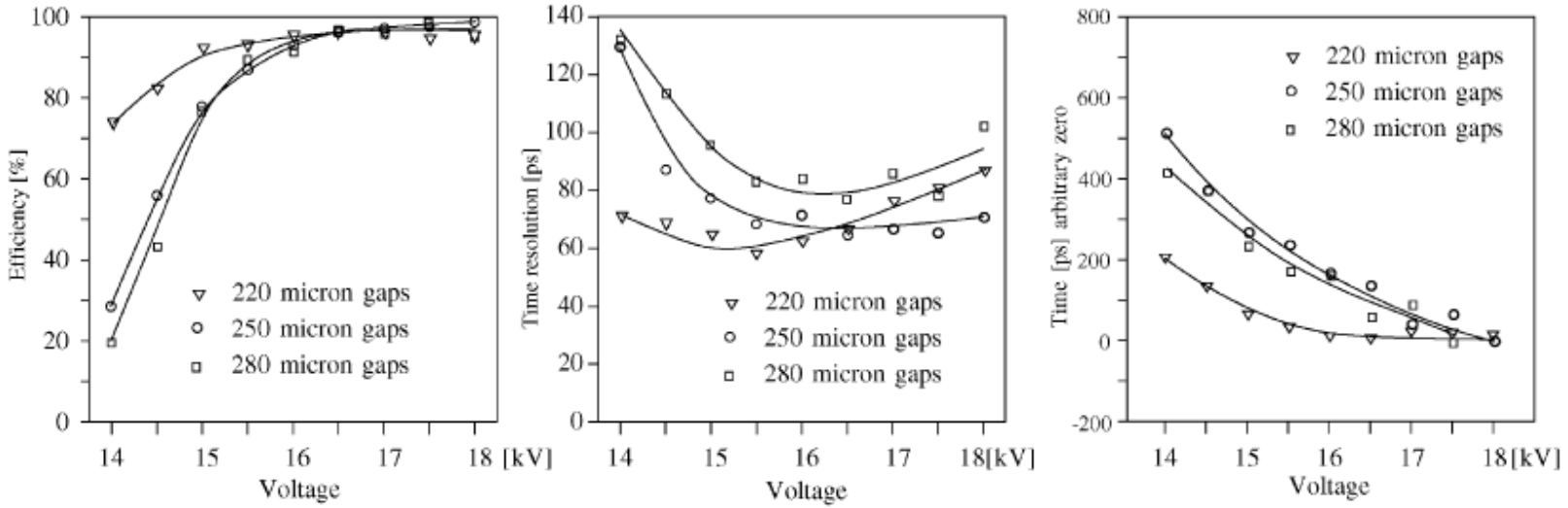

Fig. 4. Efficiency, time resolution and time walk as a function of the high voltage.

Nuclear Instruments and Methods in Physics Research A 602 (2009) 780–783

Contents lists available at ScienceDirect

Nuclear Instruments and Methods in Physics Research A

journal homepage: www.elsevier.com/locate/nima

Efficiency of RPC detectors for whole-body human TOF-PET

A. Blanco [a], M. Couceiro [a,b], P. Crespo [a], N.C. Ferreira [c], R. Ferreira Marques [a,d], P. Fonte [a,b,*], L. Lopes [a], J.A. Neves [a,d]

[a] LIP, Laboratório de Instrumentação e Física Experimental de Partículas, 3004-516 Coimbra, Portugal
[b] ISEC, Instituto Superior de Engenharia de Coimbra, 3031-199 Coimbra, Portugal
[c] IBILI, Instituto Biomédico de Investigação de Luz e Imagem, Faculty of Medicine, 3004-516 Coimbra, Portugal
[d] Departamento de Física, Universidade de Coimbra, 3004-516 Coimbra, Portugal

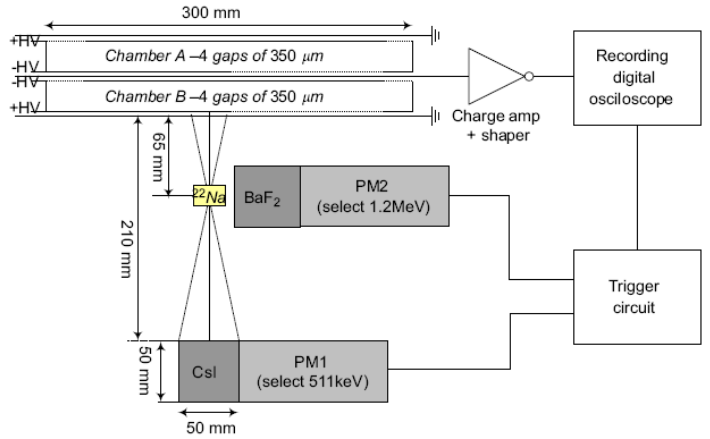

3.3. Results

Measurements were done for a set of symmetrically applied voltages from ±6.2 to ±7.0 kV, on both chambers simultaneously or on individual ones, Fig. 6.

The curves are rather flat and the error incurred on the extrapolation to zero charge is certainly small. All voltages yield essentially the same intrinsic efficiency, confirming that the result is quite independent from readout effects.

In Fig. 7, the comparison between the measurements (from Fig. 6), the measurements corrected by the setup efficiency and the simulations are shown. All voltages are shown. The corrected points lie just slightly above the simulations, mutually confirming the reliability of the results.

The detector was composed of two 5-glass stacks, forming 4+4 gas gaps of 0.35 mm width, Fig. 4. The glass thickness was 0.4 mm with the active area 30 × 30 cm^2. High voltage (HV) was applied symmetrically to the outer glasses of each stack by resistive electrically transparent [9,10] KAPTON^{TM} foils, while the intermediate glasses were left electrically floating [11]. The readout electrodes were insulated from the RPC and kept close to ground potential. The ensemble was placed in a gas-box with a thin aluminum entrance window and flushed with 90% $C_2H_2F_4$+10% SF_6.

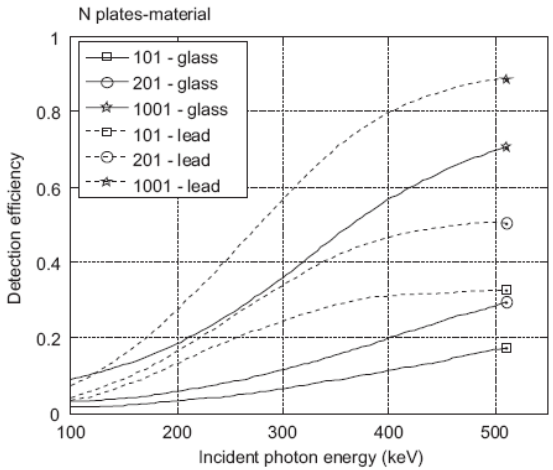

Fig. 2. Detection efficiency as a function of the incident photon energy for stacks of glass and lead optimum-thickness plates. The curves for lead-glass (not shown) are very similar to those of lead.

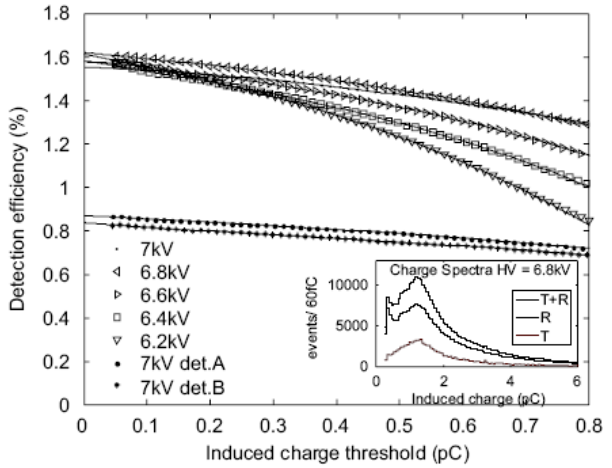

Fig. 6. Measured detection efficiency as a function of the threshold used for signal detection, converted to the charge induced on the electrodes. The interpolating cubic polynomial extrapolated to zero charge yields the intrinsic efficiency, which may be compared with the simulations. The inset shows an example of the corresponding charge distribution (see Fig. 5 for the definitions of T and R).

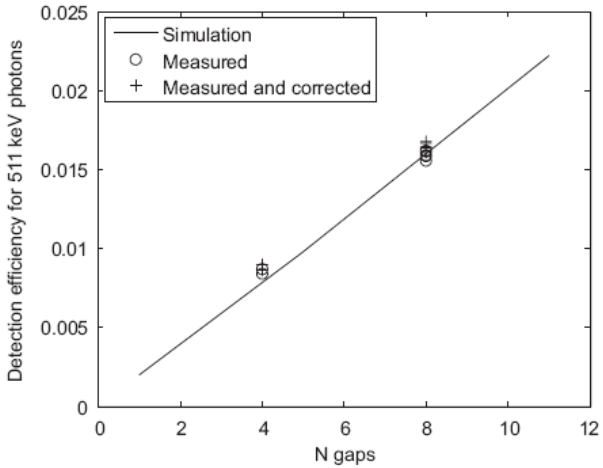

Fig. 7. Comparison between the measurements shown in Fig. 6 (all curves), the measurements corrected by the setup efficiency and the simulations, showing a very good agreement.

plates the optimum plate thickness ranges from 280 to 380 μm for